High-Resolution Historical Climate Simulations over Alaska

ANDREW J. MONAGHAN, MARTYN P. CLARK, MICHAEL P. BARLAGE, ANDREW J. NEWMAN, AND LULIN XUE

National Center for Atmospheric Research, Boulder, Colorado

JEFFREY R. ARNOLD

U.S. Army Corps of Engineers, Seattle, Washington

ROY M. RASMUSSEN

National Center for Atmospheric Research, Boulder, Colorado

(Manuscript received 8 June 2017, in final form 1 December 2017)

ABSTRACT

Weather and climate variability strongly influence the people, infrastructure, and economy of Alaska. However, the sparse observational network in Alaska limits our understanding of meteorological variability, particularly of precipitation processes that influence the hydrologic cycle. Here, a new 14-yr (September 2002–August 2016) dataset for Alaska with 4-km grid spacing is described and evaluated. The dataset, generated with the Weather Research and Forecasting (WRF) Model, is useful for gaining insight into meteorological and hydrologic processes, and provides a baseline against which to measure future environmental change. The WRF fields are evaluated at annual, seasonal, and daily time scales against observation-based gridded and station records of 2-m air temperature, precipitation, and snowfall. Pattern correlations between annual mean WRF and observation-based gridded fields are $r = 0.89$ for 2-m temperature, $r = 0.75$ for precipitation, $r = 0.82$ for snow-day fraction, $r = 0.55$ for first snow day of the season, and $r = 0.71$ for last snow day of the season. A shortcoming of the WRF dataset is that spring snowmelt occurs too early over a majority of the state, due partly to positive 2-m temperature biases in winter and spring. Strengths include an improved representation of the interannual variability of 2-m temperature and precipitation and accurately simulated (relative to regional station observations) winter and summer precipitation maxima. This initial evaluation suggests that the 4-km WRF climate dataset robustly simulates meteorological processes and recent climatic variability in Alaska. The dataset may be particularly useful for applications that require high-temporal-frequency weather fields, such as driving hydrologic or glacier models. Future studies will provide further insight on its ability to represent other aspects of Alaska's climate.

1. Introduction

Weather and climate variability strongly influence the environment and people of Alaska. Examples include modulation of boreal wildfire dynamics by summer temperatures (Balshi et al. 2009), tree damage from heavy snowfall (Sampson and Wurtz 1994), shifts in the greening of spring vegetation linked to cloud variability (Bieniek et al. 2015), the contribution of storm frequency to coastal erosion (Barnhart et al. 2014), the sensitivity of glacier mass balance to meteorological forcing (Beamer et al. 2016), variations in growing-season length as a function of temperature (Park et al. 2016), infrastructure damage due to temperature-driven permafrost degradation (Brubaker et al. 2011), and fluctuations in subsistence hunting and herding seasons due to temperature and snowfall variability (Rattenbury et al. 2009). In turn, Alaska and the Arctic are experiencing among the highest rates of climate change globally (Walsh 2014; Walsh et al. 2017). Major shifts in temperature, precipitation, snow cover, snowmelt, and streamflow have been documented in recent decades (Stafford et al. 2000; Stone et al. 2002; Wendler and Shulski 2009; Derksen and Brown 2012; Bieniek et al. 2014; Bennett et al. 2015). These changes have had widespread impacts

Corresponding author: Andrew J. Monaghan, monaghan@ucar.edu

DOI: 10.1175/JAMC-D-17-0161.1

on the environment and people of Alaska that are projected to continue into the future (Hinzman et al. 2005; Markon et al. 2012; Melvin et al. 2017).

Despite the importance of climate variability and change for Alaska, historical meteorological observations are sparse, limiting our understanding of regional variability and change (Fleming et al. 2000; Kane and Stuefer 2015). Additionally, existing meteorological records have variable quality, continuity, and length, hindering quantification of historical trends (McAfee et al. 2013; Bieniek et al. 2014). To address these issues, numerous observation-based, empirically derived gridded climate datasets have been developed for Alaska, facilitated by advancements in satellite-observing platforms and increasingly sophisticated spatial statistical approaches. Examples include ~1–2-km monthly mean temperature and precipitation (Fleming et al. 2000; Simpson et al. 2002; Hill et al. 2015; SNAP 2016), ~1-km monthly decadal mean snow/rain partitioning (McAfee et al. 2014b), and 500-m annual snow cover characteristics (Lindsay et al. 2015).

While empirically derived gridded observational datasets have greatly enhanced our knowledge of Alaska climate characteristics, they are still subject to data and methodological uncertainty, limiting their utility for assessing temporal variability and trends (e.g., McAfee et al. 2014a). Additionally, such datasets are usually restricted to time steps of months or longer and, thus, cannot typically be used to identify the underlying meteorological processes that drive variability. Therefore, global and regional meteorological model datasets, which have higher temporal resolution, have also been employed in recent years to investigate Alaska weather and climate. Global model reanalysis datasets, which assimilate historical satellite and surface-based observations, have been beneficial for gaining insight on synoptic-scale processes in Alaska (e.g., Shulski et al. 2010; E. Cassano et al. 2011, 2016; J. Cassano et al. 2016), but relatively coarse grid spacing (≥0.5°) has limited their value for understanding local-scale processes in areas of complex topography (Lader et al. 2016). For these finer scales, regional model datasets—generated by dynamically downscaling a global reanalysis (or global climate model) with a limited-area meteorological (or coupled earth systems) model—have been used. Examples of long-term regional model simulations that focused on Alaska or the Arctic in the past decade include a 10-yr, 30-km simulation over Alaska, nested to 10 km over the Alaska Range for use in glacier mass balance modeling (Zhang et al. 2007); a 31-yr, 10-km simulation using data assimilation over northern Alaska and the Chukchi–Beaufort Seas for understanding environmental changes, particularly to surface winds, in the region (X. Zhang et al. 2013; Liu et al. 2014); a 13-yr, 10 km (nested from 30 km) regional reanalysis over the circumpolar Arctic, including Alaska, for advancing high-latitude data assimilation and improving depiction of Arctic climate variability (Bromwich et al. 2016); a 19-yr, 50-km atmospheric simulation, a component of the Regional Arctic System Model, for resolving high-latitude land–atmosphere–sea ice–ocean coupling (Glisan et al. 2016; DuVivier et al. 2016); and a 35-yr, 20-km simulation over Alaska for assessing historical temperature and precipitation variability, and eventually future change (Bieniek et al. 2016).

Validation of empirical- and model-based datasets for Alaska remains a challenge, in part because the process employs most or all of the observational data that exist (leaving little independent data against which to evaluate products), and in part because there are expanses of the state where observations are virtually nonexistent (Kane and Stuefer 2015). Additionally, the station observations that do exist are skewed toward low elevations and thus high-elevation measurements are underrepresented; for example, of the 164 stations used for validation in this study, 122 are below 500 m, 37 are between 500 and 1000 m, and only 7 are above 1000 m. Therefore, an ''ensemble'' approach using numerous gridded climate datasets that employ different methodologies and data sources can be a useful means of understanding and quantifying uncertainty regarding aspects of Alaska's climate. Here, we introduce a new regional model dataset generated with the Weather Research and Forecasting (WRF) Model that complements the existing empirical- and model-based datasets described above. Unique aspects of the new WRF dataset include its combination of fine grid spacing (4 km) over a relatively long period (14 yr) and the ready availability of key model outputs at hourly temporal resolution (dataset available via Monaghan et al. 2016), enabling its use for driving downstream models (e.g., hydrologic or glacial) or for evaluating aspects of diurnally varying processes. Annual, seasonal, and daily meteorological fields from the new WRF dataset are evaluated by comparison to station records and empirically derived gridded products. The methods and data for generating and evaluating the new WRF dataset are described in section 2, the results of the model evaluation are presented in section 3, and a discussion and conclusions are provided in section 4.

2. Methods and data

a. Atmospheric model configuration

Meteorological simulations over Alaska were performed with version 3.7.1 of the Advanced Research

TABLE 1. WRF and Noah-MP parameterization options selected.

Parameterization name	Option	Option No.
WRF parameterizations		
Cloud microphysics	Thompson	8
Longwave radiation	RRTMG	4
Shortwave radiation	RRTMG	4
Surface layer	MM5 similarity	91
Surface	Noah-MP	4
Lake	FLake	1
Planetary boundary layer	Yonsei University (YSU)	1
Cumulus	Off	0
Noah-MP parameterizations		
Dynamic vegetation (dveg)	Off	4
Stomatal resistance (opt_crs)	Ball–Berry	1
Surface layer drag coefficient (opt_sfc)	Monin–Obukhov	1
Soil moisture factor for stomatal resistance (opt_btr)	Noah	1
Runoff (opt_run)	Original surface/subsurface runoff	3
Supercooled liquid water (opt_frz)	No iteration	1
Soil permeability (opt_inf)	Linear effect	1
Radiative transfer (opt_rad)	Two-stream method applied to vegetated fraction	3
Ground surface albedo (opt_alb)	Canadian Land Surface Scheme	2
Precipitation (snow/rain) partitioning (opt_snf)	Snow when SFCTMP < TFRZ	3
Soil temperature lower boundary (opt_tbot)	Zero heat flux	1
Soil/snow temperature time scheme (opt_stc)	T_ground weighted using snow fraction	3

WRF (Skamarock et al. 2008). WRF is a fully compressible conservative-form nonhydrostatic atmospheric model suitable for both research and weather prediction applications at a variety of spatial and temporal scales (Klemp et al. 2007; Skamarock and Klemp 2008). WRF has multiple options for physical parameterizations of radiation, cloud microphysics, cumulus clouds, surface and planetary boundary layer turbulence, and inland lake dynamics that are specified by the user depending on the application. Here, WRF is coupled to the Noah multiparameterization land surface model (Noah-MP; Niu et al. 2011) in order to simulate two-way land–atmosphere interactions. Noah-MP provides WRF with fluxes of energy and moisture from the land surface and maintains stores of water and energy in four soil layers to a depth of 2 m.

WRF and Noah-MP parameterizations used for the simulations are summarized in Table 1. The parameterizations were selected by running year-long simulations with various model configurations based on WRF configurations used in prior applications over Alaska, the Arctic, or midlatitude mountain regions (J. Cassano et al. 2011; Rasmussen et al. 2011; Gong et al. 2013; Bieniek et al. 2016; Bromwich et al. 2016). Results from the different simulations were compared to temperature, precipitation, and snow water equivalent (SWE) observations at Snowpack Telemetry (SNOTEL) sites across Alaska (SNOTEL observations are described below). Parameters from those simulations most accurately simulating the SNOTEL variables were then combined iteratively in subsequent simulations to arrive at the optimal WRF parameter set described in Table 1.

A number of modifications were made to the Noah-MP parameter file MPTABLE.TBL to improve treatment of seasonal snowpack evolution and, particularly, to alleviate an early melt bias in the year-long test simulations during springtime. First, the parameter determining the snow depth to snow cover relationship (MFSNO) was decreased to 1.0 from the default of 2.5 for all land-use types to allow greater snow cover fraction at the beginning and end of winter season when snow is patchy and may be melting. Niu and Yang (2007) noted that MFSNO is scale dependent and should be lower for finer spatial resolutions. Second, the liquid water holding capacity for snowpack (SSI) was increased to $0.06\,m^3\,m^{-3}$ from the default of $0.03\,m^3\,m^{-3}$ to allow the snow to ripen for a longer period before melt runoff occurs. Third, the canopy wind absorption coefficient (CWPVT) was changed from a constant value of 0.18 for all land-use types to a variable ranging from 0.18 up to 5.00 [with rougher surfaces having the highest values; Goudriaan (1985)]. This change more realistically represents the heterogeneity among vegetation types and acts to reduce below-canopy wind speed and turbulent exchanges and generally decrease melt. Finally, the monthly varying LAI values for woody savannah and savannah land-use types were modified to better represent the characteristics of evergreen needleleaf trees characteristic of Alaska. In the default model the savannah land-use types are based on midlatitude deciduous trees that have no foliage during the cold season.

Two bugs were also discovered and fixed, and both fixes have since been implemented in the official release of WRF, version 3.8. First, a bug was fixed in the opt_stc option of Noah-MP that effectively caused opt_stc = 3 to reproduce opt_stc = 1 results. Second, a bug was fixed in the radiation driver module that caused excessive cloud estimates when Thompson microphysics, Rapid Radiative Transfer Model for GCMs (RRTMG) radiation, and (icloud = 3) were used in combination. The icloud = 3 option follows Sundqvist et al. (1989) and was a new addition as of WRF, version 3.7, intended to alleviate the persistent tendency toward binary cloud fraction values (0 or 1) when using the icloud = 1 option.

A one-domain 4-km WRF configuration was employed (Fig. 1). A grid spacing of 4 km was chosen based on previous work by Prein et al. (2013) demonstrating that 4-km WRF simulations had markedly improved spatial patterns of heavy precipitation in complex topography compared to coarser (12 and 36 km) grid spacings; similarly, Rasmussen et al. (2011) showed that snowfall was best represented at WRF grid spacing <6 km. Static data inputs included terrain elevation from the U.S. Geological Survey (USGS) 30 arc-s GTOPO30 dataset (Gesch and Greenlee 1999) and the 20-category land-use information from the Moderate Resolution Imaging Sprectroradiometer (MODIS) IGBP dataset (Friedl et al. 2002). There were 49 vertical levels from the surface to 30 hPa, with 7 levels in the lowest 1000 m. Initial and boundary conditions were provided by the European Centre for Medium-Range Weather Forecasts (ECMWF) interim reanalysis (ERA-Interim; Dee et al. 2011). ERA-Interim is considered one of the most accurate global atmospheric reanalyses presently available (see, e.g., Lorenz and Kunstmann 2012). More directly relevant for this study, ERA-Interim is among the top-performing reanalyses over the Arctic compared to observations of surface temperatures, radiative fluxes, precipitation, and wind speed (Lindsay et al. 2014). When considered for all of Alaska, ERA-Interim has relatively low biases and root-mean-square errors for temperature and precipitation as compared to other reanalyses for Alaska (Lader et al. 2016). Daily updated 0.01° (resampled to 0.04°) sea surface temperature (SST) and sea ice concentration (SIC) data for the oceans were specified with version 4.1 of the Multiscale Ultrahigh Resolution (MUR) SST analysis (NASA JPL 2015). Inland lake temperatures and lake ice coverage were simulated using the Freshwater Lake (FLake) model available in WRF (Mallard et al. 2014).

To spin up the land surface state, the WRF simulations were run for a 14.5-month period from 1 June 2002 to 15 August 2003. The resulting spun-up land-surface fields (subsurface temperature, soil moisture, canopy water, and skin temperature) were then used to initialize the final simulation, which was run continuously from 15 August 2002 through 31 August 2016. Throughout the simulation the WRF lateral boundaries were updated every 6 h with the ERA-Interim 3D temperature, humidity, wind, and geopotential fields; the lower boundary was updated daily with the MUR SST and SIC fields described above. The latter half of August 2002 was discarded to allow about 2 weeks for spinup of the hydrologic cycle. Hence, the final simulation analyzed here spans 1 September 2002–31 August 2016, a 14-yr period. The beginning year of the period 2002 was chosen because this is the first year the MUR SST and SIC fields became available. The first day of September, rather than the first day of the calendar year, was chosen to optimally resolve the hydrologic year, which encompasses one complete cycle of autumn and winter snowfall accumulation followed by spring and summer snowfall ablation. Key meteorological outputs were saved at 1-hourly intervals for analysis.

b. Data and methods for WRF evaluation

1) GRIDDED TEMPERATURE AND PRECIPITATION FIELDS (SNAP)

To evaluate the spatial distribution of the 2-m air temperature and precipitation amount in WRF, historical monthly temperature and precipitation fields for 2002–09 on a 2-km grid covering Alaska were obtained from the Scenarios Network for Arctic and Alaska Planning (SNAP) dataset (SNAP 2016). The historical SNAP data were generated by calculating monthly anomaly fields versus a 30-yr baseline period (1971–2000) from 0.5° Climatic Research Unit (CRU) v3.1 gridded monthly temperature and precipitation observations (Harris et al. 2014), and then employing a delta approach (e.g., Jones 1994) to downscale these 0.5° anomaly fields using 2-km monthly fields from the Parameter-Elevation Regression on Independent Slopes Model (PRISM) climatology averaged for the same 30-yr baseline period (Daly et al. 1994; Simpson et al. 2002, 2005). An additional product available in the SNAP database, mean snow-day fraction for 2000–09 (McAfee et al. 2014b), was employed to evaluate the precipitation phase (snow–rain partitioning) in WRF. The SNAP snow-day fraction was diagnosed as a function of monthly average temperature based on observational data, and then gridded by applying the diagnostic fits to CRU and PRISM fields. Additional information on methods and uncertainty for the SNAP fields may be found in McAfee et al. (2014b) and SNAP (2016).

The total all-type grid-scale precipitation (RAINNC) and 2-m temperature (T2) from WRF were compared to

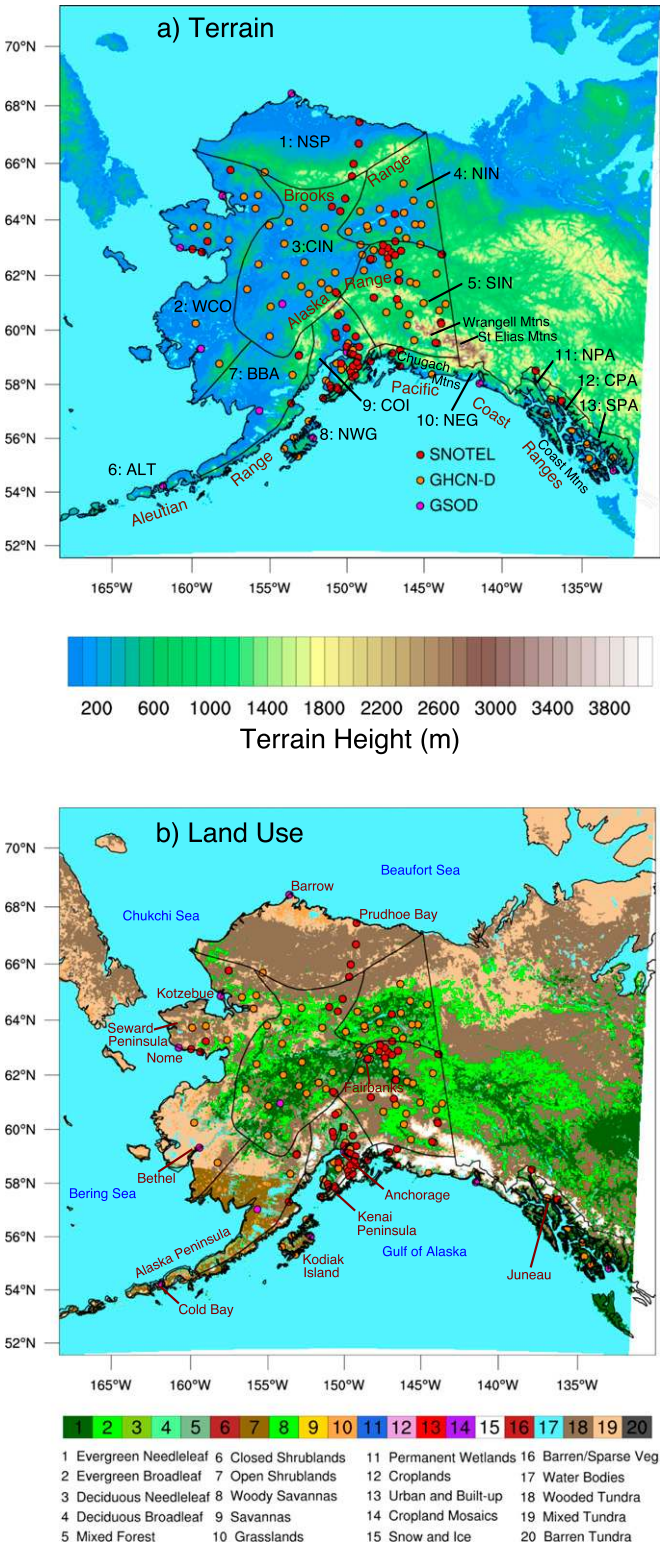

FIG. 1. WRF (a) terrain height and (b) land-use categories. Station data used for model evaluation are indicated by color-filled circles. The 13 Alaska climate divisions (Bieniek et al. 2012) are delineated by black lines: 1, North Slope (NSP); 2, west coast (WCO); 3, central interior (CIN); 4, northeast interior (NIN); 5, southeast interior (SIN); 6, Aleutians (ALT); 7, Bristol Bay (BBA); 8, northwest gulf (NWG); 9, Cook Inlet (COI); 10, northeast gulf (NEG); 11, north panhandle (NPA); 12, central panhandle (CPA); and 13, south panhandle (SPA).

the SNAP precipitation and temperature fields (note that the convective parameterization in WRF was turned off because convection is explicitly simulated as grid-scale precipitation at 4-km grid spacing, so it was unnecessary to use the RAINC variable). The WRF snow-day fraction field (SDF) was developed using Eq. (1) from McAfee et al. (2014b), in which the numbers of snowy days (nsd), mixed precipitation days (nmd), and wet days (nwd) were calculated for each year y and month m, and then the snow-day fraction was calculated as

$$\mathrm{SDF}_{m,y} = (\mathrm{nsd}_{m,y} - \mathrm{nmd}_{m,y})/\mathrm{nwd}_{m,y}, \qquad (1)$$

that is, after removing the mixed precipitation days from consideration, the monthly SDF was the ratio of snow-only days to all-type precipitation days. For WRF a snowy day had snowfall > 0.1 mm water equivalent (weq). A mixed precipitation day had both snowfall > 0.1 mm weq and rainfall > 0.1 mm weq. A wet day had any type of precipitation > 0.1 mm weq. A cutoff value of 0.1 mm was used because McAfee et al. (2014b) used cutoff values of 0.1 mm for rain and 1 mm for snow depth; because WRF snowfall units are in mm weq, not mm depth, we used a cutoff of 0.1 mm for snow, assuming the density of fresh snow is about 10% of water, or 100 kg m^{-3} (Kienzle 2008). Results are nearly identical when testing the algorithm using a cutoff of 1 mm weq. Monthly results were aggregated into long-term annual and seasonal means for 2003–12 for comparison to the 2000–09 snow-day product of McAfee et al. (2014b); 2003–12 was the 10-yr period in the WRF output nearest to 2000–09. For direct comparison with WRF, all SNAP data were bilinearly interpolated to the 4-km WRF domain.

2) MODIS SNOW COVER METRICS (GINA)

To spatially evaluate WRF annual snow cover characteristics, the 500-m MODIS-derived snow cover metrics (Lindsay et al. 2015) were obtained from the Geographic Information Network of Alaska for 2002–16 (GINA 2016). The MODIS-derived snow cover metrics (henceforth referred to as GINA), developed by the U.S. Department of the Interior/National Park Service, were compiled from the MODIS *Terra* Snow Cover Daily L3 Global 500-m Grid dataset (MOD10A1), infilled to account for clouds and polar darkness (Lindsay et al. 2015). WRF outputs were compared to two metrics: the first snow day of the full season (FSD) and the last snow day of the full season (LSD). Compared to in situ SNOTEL observations, there is an early bias in GINA for the first day of the snow season of about 11–22 days depending on land-use type (Lindsay et al. 2015). The bias for the last day of the snow season is about 1–4 days early; more discussion of this bias appears below.

The snow cover fraction variable (SNOWC) was used to generate the WRF metrics for comparison to GINA. If SNOWC > 0.0 at the end of any day for a given grid box, it was considered a snow day (SD). The results were similar when testing using a threshold of SNOWC ≥ 0.5. The WRF FSD was the first SD of the given "snow year," which spans 1 August–31 July, following Lindsay et al. (2015). Similarly, the WRF LSD was the last SD of a snow year. For comparison with WRF, all GINA data were bilinearly interpolated to the 4-km WRF domain.

3) STATION DATA FROM SNOTEL GHCN-D AND GSOD

Station observations were used to evaluate WRF fields at sites across Alaska at annual, seasonal, and daily time scales (Fig. 1). Daily historical near-surface air temperature, precipitation, and SWE measurements for 2002–16 from the SNOTEL network (Schaefer and Paetzold 2000) were obtained from the Natural Resources Conservation Service (NRCS) of the U.S. Department of Agriculture (NRCS 2016). Daily historical near-surface air temperature and precipitation measurements for the same period were obtained from the Global Historical Climatology Network – Daily (GHCN-D) database housed at the National Oceanic and Atmospheric Administration's (NOAA) National Centers for Environmental Information (Menne et al. 2012a,b), and the Global Surface Summary of the Day (GSOD) database (NOAA/NCEI 2016).

The SNOTEL sites employ snow pillow pressure transducers to measure SWE, sonic sensors for snow depth, and standard 12-in.-orifice shielded all-season gauges for precipitation amount. Air temperature is measured with shielded thermistors. SNOTEL data are quality controlled by comparing manually measured and telemetered readings during regularly scheduled maintenance surveys, and values beyond specified limits are examined and edited to maintain a high quality record (NRCS 2017). The accuracy of SWE measurements may be lower for periods of rapid melting, melting of thin snow, and rapid snow settlement (Johnson et al. 2007). Undercatch can affect precipitation amount (particularly snowfall) measurements and is related to wind speed (Yang et al. 1998). The GHCN-D and GSOD records come from various types of stations and instruments (Menne et al. 2012b). Extensive quality assurance checks for GHCN-D and GSOD were applied by NOAA prior to distribution via the method of Durre et al. (2010), which incorporates 19 tests that detect duplicates, outliers, and internal, spatial, and temporal inconsistencies. These data were not adjusted to account

for artifacts associated with changes in instrumentation or reporting practices. No additional quality control of the precipitation and SWE fields (where available) from the SNOTEL, GHCN-D, and GSOD observations was performed for the present analysis. However, visual inspection indicated the presence of occasional erroneous values of daily average near-surface air temperature at some stations; these values were removed if they differed by >20°C from the WRF 2-m air temperature value (bilinearly interpolated to the site coordinates) for the same day (spurious points removed by this method represent <1% of the dataset).

WRF 2-m temperature, rainfall and snowfall, snow cover, and SWE fields were bilinearly interpolated to the location of each SNOTEL, GHCN-D, and GSOD station for comparison over the 2002–16 period (henceforth we refer to the station observations collectively as OBS). Comparisons between WRF and OBS were only made for days on which observations were available; for example, if only 27 days of OBS were available for a given month, the WRF monthly mean was computed based on those 27 days. Monthly means were only calculated if > 25 days of data were available. Likewise, seasonal and annual means were only calculated if all monthly means were available for a given period. Seasonal means were calculated for winter [December–February (DJF)] and summer [June–August (JJA)]. Long-term average values were computed if at least 5 yr of annual or seasonal values were available for a given station (this was done to allow for the robust calculation of standard deviations and bias statistics, which were based on the computed means). The SDF was computed from the OBS, but because mixed precipitation could not be distinguished for stations that do not measure both rainfall and snowfall following the methodology described above for SNAP and that used in McAfee et al. (2014b), SDF was estimated as the ratio of all snowfall days to all precipitation days for a given year or season. A day was considered a snowfall day if precipitation occurred and the mean 2-m temperature on that day was <0°C (see Dai 2008 and references within). This temperature threshold method was used because the OBS do not distinguish between rainfall and snowfall. For direct comparison, WRF snow-day fraction was computed in the same manner. While this method is imperfect, it is noteworthy that SDF biases for WRF compared to OBS are similar to those computed for WRF compared to SNAP (shown below in section 3).

c. *Overview of study region*

Alaska has numerous mountain ranges with primarily east–west orientations (Fig. 1a). The Brooks Range is farthest north and separates the North Slope from the interior. The Alaska Range lies to the south of the Brooks Range and largely separates the interior from southern Alaska. South of the Alaska Range, the Pacific Coast Ranges bound the southeastern and south-central reaches of the state and include the Chugach, Wrangell, St. Elias, and Coast Mountains. The Aleutian Range forms the backbone of the Alaska Peninsula and Aleutian Islands in southwestern Alaska. Mountains play a first-order role in defining the climate zones of Alaska (Bieniek et al. 2012), as noted in the results presented below. Vegetation is characterized by temperate rain forests in southeastern Alaska, glaciers throughout the coastal mountains and Alaska Range, evergreen forests in the interior, and open shrublands and tundra in the western and northern reaches of the state (Fig. 1b).

3. Results

a. *Evaluation of annual and seasonal 2-m temperature*

WRF simulates the broad spatial patterns of annual, winter (DJF), and summer (JJA) mean 2-m temperature compared to SNAP (Fig. 2), with Spearman rank-order correlation coefficients between WRF and SNAP patterns of 0.89, 0.89, and 0.80 for the three respective periods (Table 2). Temperatures generally increase from north to south; an exception is during summer, when the interior of Alaska has the highest temperatures because of its continentality (Fleming et al. 2000). Annually, temperature differences between WRF and SNAP are generally ±2°C; differences of less than ~1°C are not statistically significant (the statistical significances of all differences calculated in this paper are assessed using the Student's t test). During winter, WRF is warmer than SNAP by up to 5°C across the Brooks Range and throughout much of the interior and south-central portions of the state east of the Kenai Peninsula. In summer, WRF is generally colder than SNAP across most of Alaska. In western and southeastern Alaska, WRF is colder than SNAP annually and in winter and summer. Grid-averaged differences between WRF and SNAP are −0.73°C (annual), +0.87°C (DJF) and −1.78°C (JJA) (Table 2). When WRF is compared to OBS, the spatial patterns and magnitude of the temperature differences are similar to those for WRF versus SNAP, though many of the differences are not statistically significant. Some biases, particularly in regions of complex topography, are partly due to elevation differences between WRF and OBS (this topic is addressed further in section 4).

WRF and SNAP have somewhat different patterns of interannual variability of annual, winter, and summer 2-m temperature, as indicated by the standard deviation (Fig. 3), and comparatively lower pattern correlations

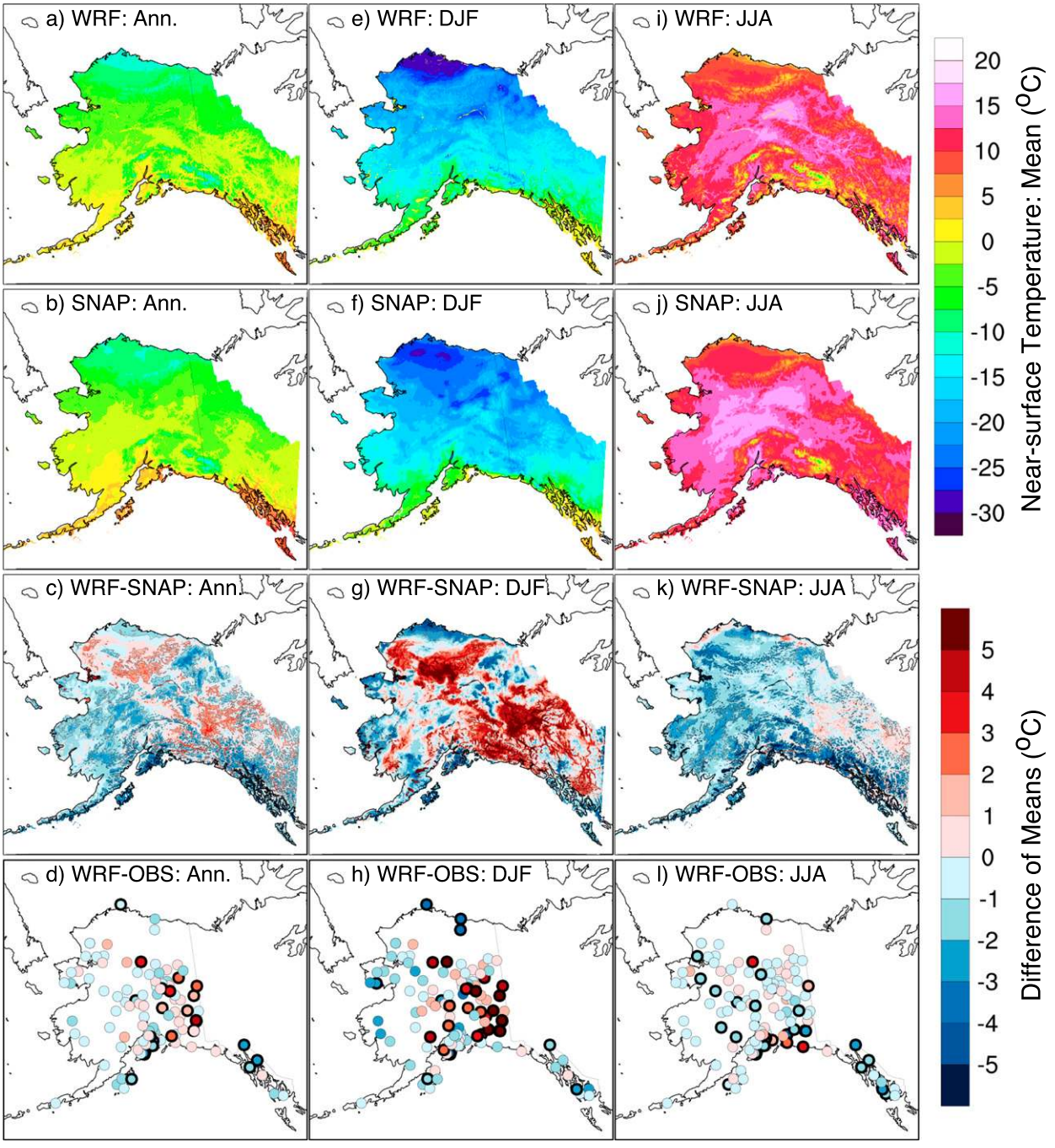

FIG. 2. Comparison of mean 2-m air temperature between WRF, SNAP, and OBS. Shown are (a),(e),(i) WRF 2002–09 means, (b),(f),(j) SNAP 2002–09 means, (c),(g),(k) WRF minus SNAP, and (d),(h),(l WRF minus OBS for (left) annual, (center) DJF, and (right) JJA results. The results for WRF and SNAP are compared for 2002–09 whereas those for WRF and OBS are compared for 2002–16. Statistically significant differences ($p < 0.05$) between WRF and SNAP are outlined in thin gray contours in (c), (g), and (k). Statistically significant differences between WRF and OBS are indicated by boldface-outlined circles in (d), (h), and (l).

(Table 2). While annual patterns are broadly similar (r = 0.63) and indicate lower variability in the north, and higher variability in western–southwestern Alaska, the winter and summer patterns are less similar. The spatial patterns of interannual temperature variability in SNAP appear to be associated with proximity to the station data that provide constraint; for example, in winter, there is a ''bull's eye'' emanating from Barrow (the northernmost

TABLE 2. Gridwide differences and Spearman rank-order correlation coefficients for WRF compared with SNAP (Figs. 2–6) and GINA (Figs. 7 and 8). Statistically significant values ($p < 0.001$) are set in boldface. Insignificant values ($p > 0.05$) are set in italics.

Variable	Units	Difference (WRF minus SNAP or GINA)			Spearman rank-order correlation		
		Annual	DJF	JJA	Annual	DJF	JJA
Mean 2-m temperature (Fig. 2)	°C	**−0.73**	**0.87**	**−1.78**	**0.89**	**0.89**	**0.80**
Std dev of 2-m temperature (Fig. 3)	°C	**0.07**	**−0.18**	**0.62**	**0.63**	**0.55**	**0.35**
Mean precipitation (Fig. 4)	mm weq	**−58.28**	**−3.98**	**−29.27**	**0.75**	**0.74**	**0.62**
COV of precipitation (Fig. 5)	%	**−1.61**	**−0.29**	**0.32**	**0.10**	**0.08**	**0.18**
Mean SDF (Fig. 6)	%	**−5.45**	*−0.12*	**−2.08**	**0.82**	**0.76**	**0.59**
Mean FSD (Fig. 7)	Day of year	**4.90**	—	—	**0.55**	—	—
Std dev of FSD (Fig. 8)	Days	**−5.07**	—	—	**0.07**	—	—
Mean LSD (Fig. 7)	Day of year	**−9.17**	—	—	**0.71**	—	—
Std dev of LSD (Fig. 8)	Days	**−5.67**	—	—	**0.12**	—	—

point in Alaska), as well as from near Dawson City (in Yukon, Canada, just east of the interior Alaska border). By contrast, the spatial patterns of interannual variability in WRF appear to be more closely associated with geographic features such as mountains and oceans. When averaged over the grid, WRF and SNAP have similar interannual variabilities of 2-m temperature annually and in winter; however, the WRF standard deviation is +0.62 higher than SNAP on average during summer (Table 2) and is also higher compared to most JJA OBS.

b. *Evaluation of annual and seasonal precipitation*

WRF simulates the broad spatial patterns of annual, winter, and summer mean precipitation compared to SNAP (Fig. 4), with Spearman rank-order correlation coefficients between WRF and SNAP patterns of 0.75, 0.74, and 0.62 for the three respective periods (Table 2). Annual precipitation maxima in excess of 5000 mm weq yr^{-1} occur in many regions of the Pacific Coast Ranges in south-central and southeast Alaska. WRF is drier than SNAP throughout this coastal region, though compared to the OBS it has both wet and dry biases that are partly related to elevation differences between stations and WRF grid points (this issue is elaborated upon in section 4). Annual precipitation minima below 300 mm weq yr^{-1} occur along the northern coast and in the interior to the south and east of the Brooks Range. WRF is wetter than SNAP in these regions and is wetter compared to the OBS as well. WRF is generally wetter than SNAP throughout interior Alaska, whereas it is drier than SNAP throughout much of western Alaska, except in coastal regions where it is wetter. Similarly, compared to OBS the mean annual precipitation in WRF is generally wetter in interior and coastal western Alaska (though it is not statistically significantly different from OBS at any interior sites). Seasonally, in both WRF and SNAP the southern coastal mountains receive more precipitation in winter compared to summer, whereas interior, northern, and western Alaska receive more precipitation in summer. Compared to both SNAP and OBS, the spatial patterns of differences with WRF in both summer and winter are similar to the annual differences. Grid-averaged differences between WRF and SNAP are −58 mm weq (annual), −4 mm weq (DJF), and −29 mm weq (JJA) (Table 2); the lower values in WRF are primarily attributable to lower precipitation in the southern coastal mountains.

WRF and SNAP have markedly different patterns of interannual variability of annual, winter, and summer mean precipitation (Fig. 5), which (because of the large spatial variability in precipitation magnitude) is measured using the coefficient of variation (COV). The COV is defined as the standard deviation expressed as a percentage of the mean. Low Spearman rank-order correlations of 0.10 (annual), 0.08 (DJF), and 0.18 (JJA) confirm the differences. As was the case for 2-m temperature, the patterns of interannual precipitation variability in SNAP appear to be associated with the proximity to the station data that provide constraint. The grid-averaged differences of COV (−1.61%, annual; −0.29%, DJF; and +0.32%, JJA) appear to largely reflect differences that arise due to the SNAP interpolation methodology. Compared to OBS, WRF has both positive and negative COV differences, though most WRF COVs are lower. An interesting area of comparatively high interannual winter precipitation variability is evident in WRF on the lee side of the Wrangell and St. Elias Mountains (the dark blue area in Fig. 5e). Inspection of the differences between WRF and OBS in this region (Fig. 5h) indicates that, if anything, WRF underestimates the interannual variability here. While this is an area of low total winter precipitation that may make the COV more sensitive to small year-to-year changes (Fig. 4e suggests mean winter precipitation is <50 mm weq), there are other regions in interior and northern Alaska with similar magnitudes of winter precipitation, but much lower COVs. The causality of

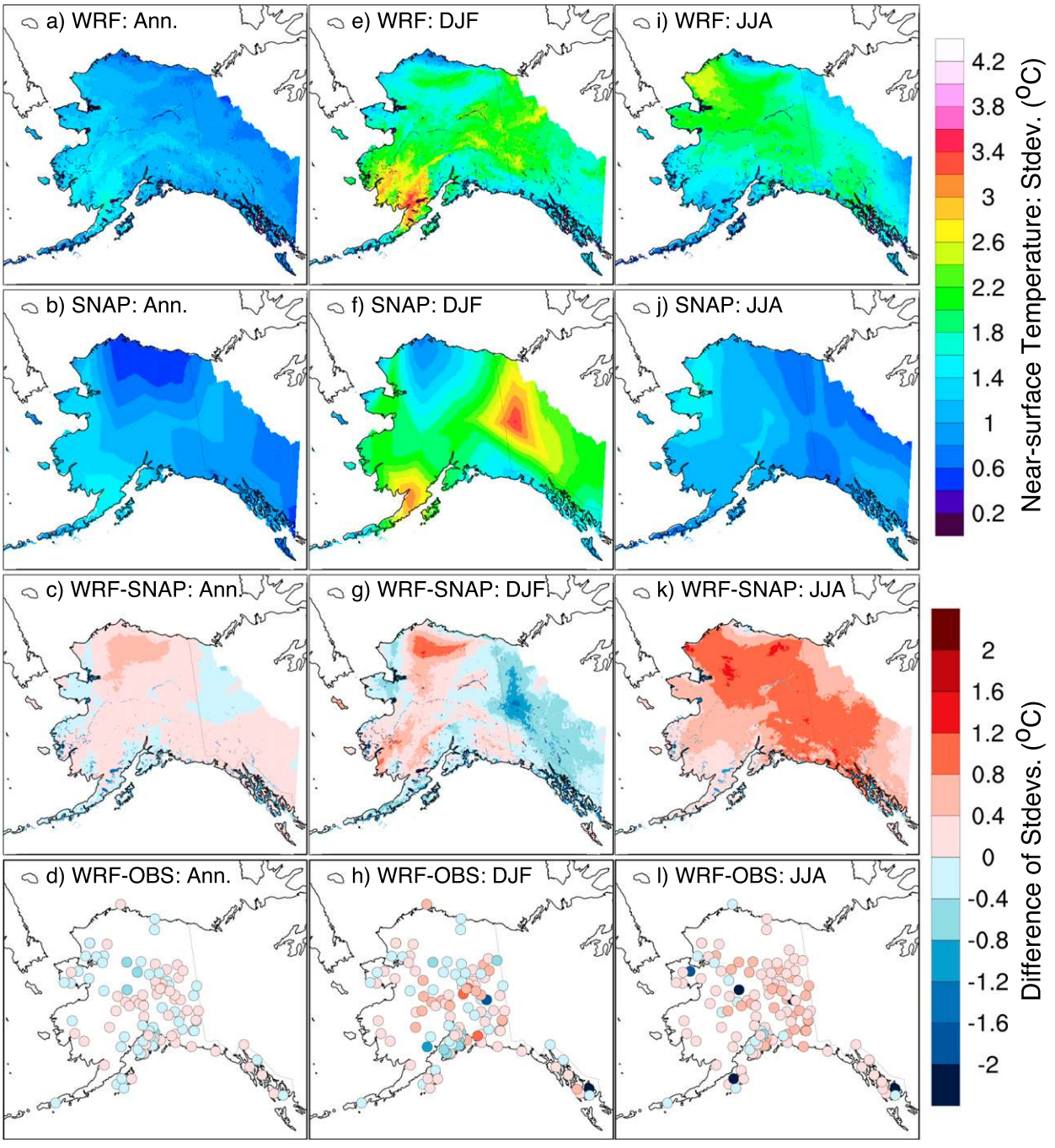

FIG. 3. Comparison of the standard deviation of mean 2-m air temperature between WRF, SNAP, and OBS. Conventions are as in Fig. 2, with the exception that the statistical significance of differences cannot be computed since many multiyear samples (i.e., an ensemble of WRF simulations) would be required to do so.

anomalously high interannual winter precipitation variability in this region will be investigated in the future.

c. *Evaluation of annual and seasonal snow–rain partitioning*

WRF simulates the broad spatial patterns of annual, winter, and summer mean SDF compared to SNAP (Fig. 6), with Spearman rank order-correlation coefficients between WRF and SNAP patterns of 0.82, 0.76, and 0.59 for the three respective periods (Table 2). Annually, SDF is highest in northern Alaska (precipitation falls as snow on >55% of days) and in the mountains; SDF is lowest in the lower-elevation coastal regions in southwest, south-central, and southeast Alaska. In winter

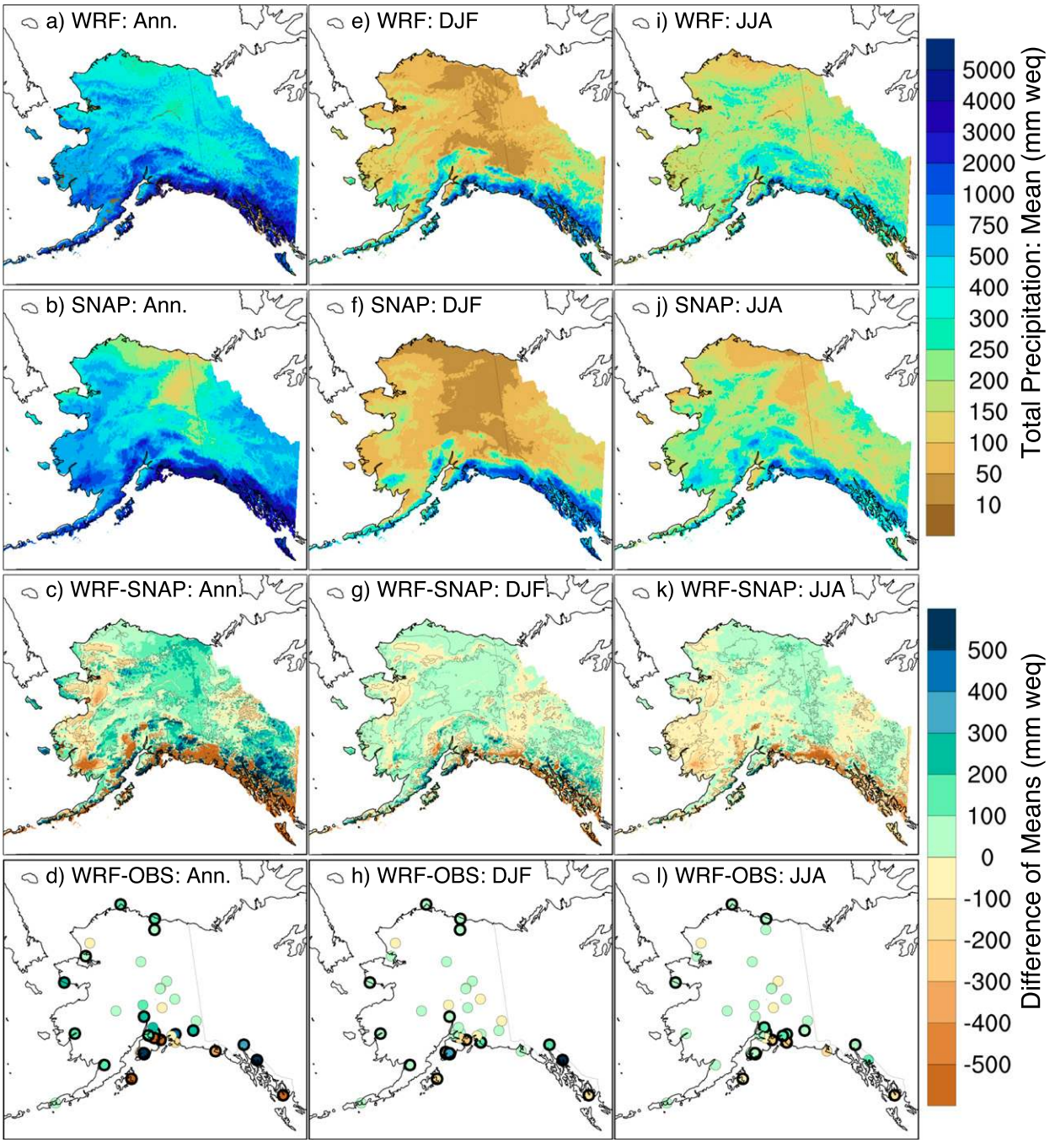

FIG. 4. Comparison of mean precipitation amounts between WRF, SNAP, and OBS. Conventions are as in Fig. 2.

precipitation falls as snow on nearly all days in the northern and interior regions; however, in the coastal southwestern, south-central, and southeast regions precipitation falls as snow on <75% of days. During the summer, precipitation falls as snow occasionally in the mountains and along the northern coast. Compared to SNAP, WRF generally has lower SDF in lower accumulation areas in interior, northern, and western Alaska, and higher SDF in the high accumulation regions of southern Alaska (though coastal areas of southeast Alaska have lower SDF in WRF). Grid-averaged differences between WRF and SNAP are −5.45% (annual), −0.12% (DJF), and −2.08% (JJA), with the difference for winter being statistically insignificant (Table 2); the lower overall SDF in WRF is driven by negative differences between WRF and SNAP

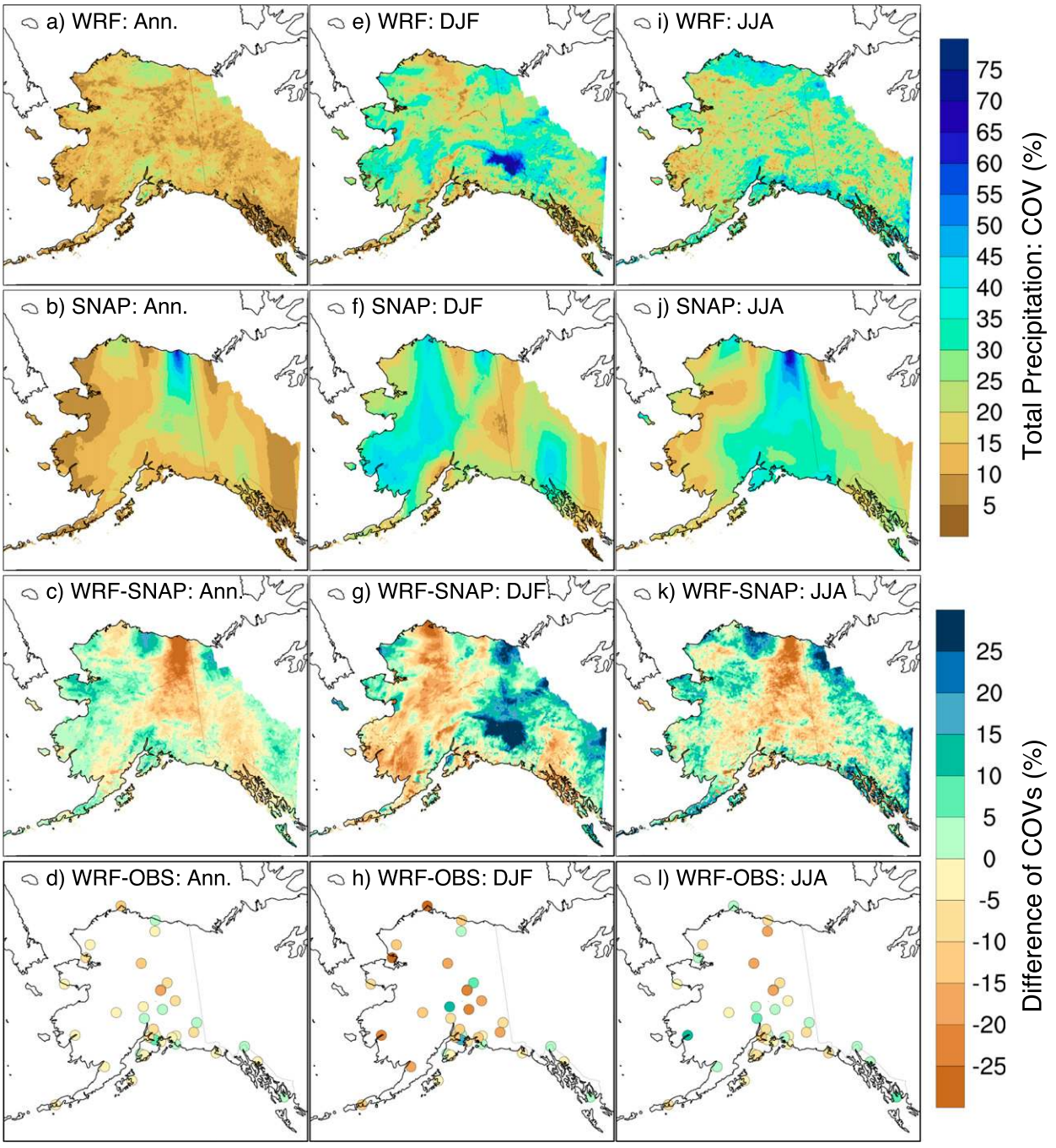

FIG. 5. Comparison of the COV of mean precipitation amount between WRF, SNAP, and OBS. Conventions are as in Fig. 2, with the exception that the statistical significance of differences cannot be computed.

in southwest Alaska and coastal southeast Alaska. Compared to OBS, WRF generally has differences < 5% at many sites; most of the larger differences indicate that WRF has higher-than-observed SDF. At the few sites available in southwestern Alaska, a region where WRF has lower SDF than SNAP, WRF differs from OBS by <5%, or has higher SDF than OBS, suggesting the WRF results are more accurate than SNAP in this region. A ''rainy'' bias in SNAP SDF in southwestern Alaska was also noted by McAfee et al. (2014b) and was attributed to the elevated sensitivity of snow-day estimates to small temperature changes for the range of temperatures encountered there.

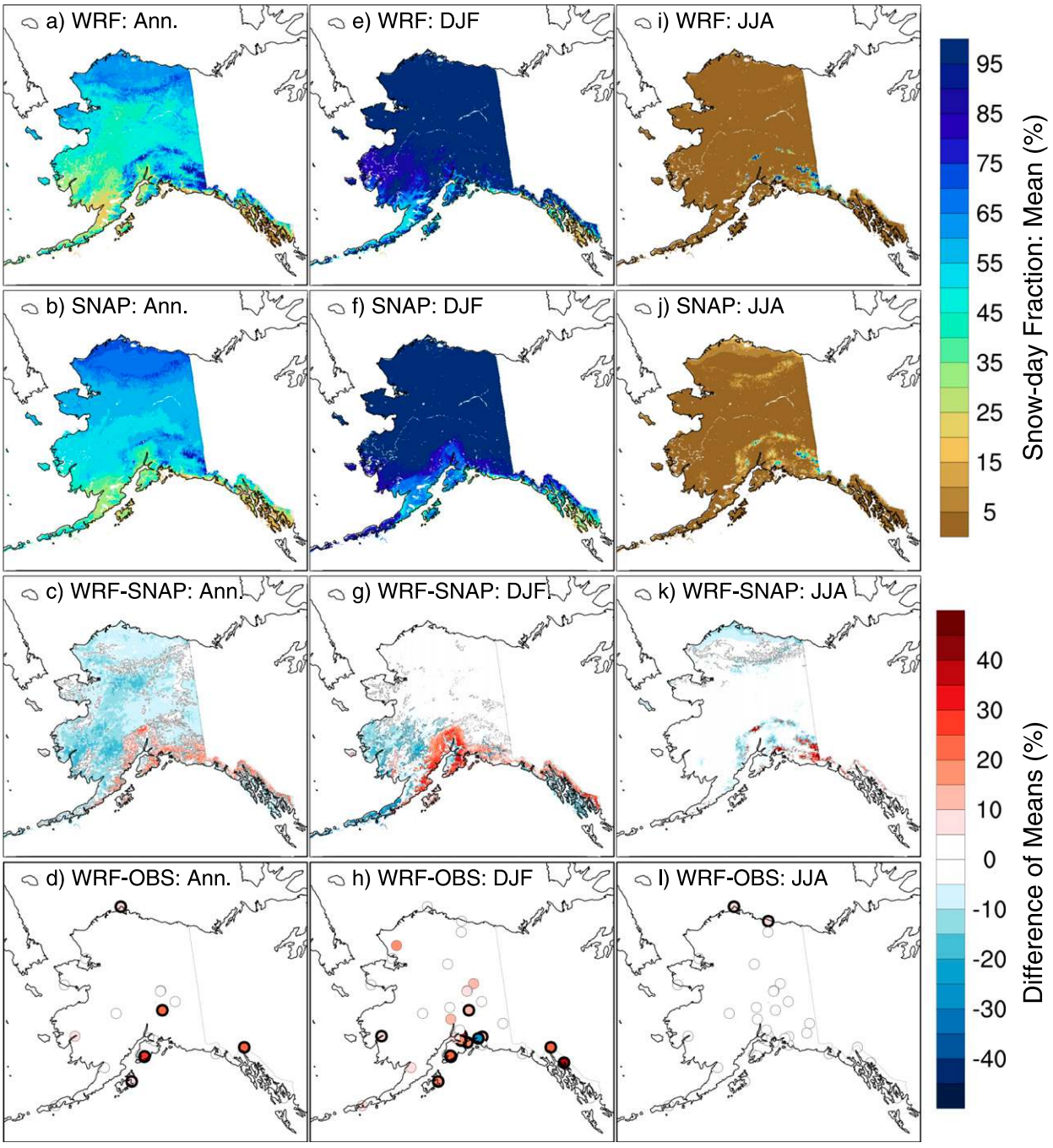

FIG. 6. Comparison of mean SDF between WRF, SNAP, and OBS. Conventions are as in Fig. 2, with the exception that the WRF results are for 2002–12 and the SNAP results are for 2000–09.

d. Evaluation of annual first and last days of snow cover

WRF simulates the broad spatial patterns of annual FSD and LSD compared to GINA (Fig. 7), with Spearman rank-order correlation coefficients between WRF and GINA patterns of 0.55 (FSD) and 0.71 (LSD) (Table 2). Inspection of the differences indicates that, on average, WRF has a later FSD and earlier LSD than GINA, and therefore a shorter snowfall season in general. Grid-averaged differences between WRF and GINA confirm this: WRF FSD is 4.90 days later on average, and WRF LSD is 9.17 days sooner. The later FSD

in WRF appears to be more consistent with OBS (which indicate no statistically significant difference from WRF except at two coastal sites), and with the assessment of Lindsay et al. (2015), who found that the GINA data were biased early compared to in situ observations. However, the earlier LSD in WRF appears to be anomalous, as both OBS and GINA indicate that the WRF snow cover melts too early in general, except in high snowfall accumulation areas in the mountains. Possible reasons for the early snowmelt bias in WRF are explored in section 4.

WRF and GINA visually have broadly similar patterns of interannual variability for FSD and LSD (measured as the standard deviation of FSD and LSD across 13 yr; Fig. 8), indicating the highest interannual variability for both FSD and LSD occurs in nonglaciated mountain regions. However, low Spearman rank-order correlations of 0.07 (FSD) and 0.12 (LSD) indicate that the patterns are not as similar as they appear (Table 2). This dissimilarity may be partly due to the noisier spatial patterns in the GINA data, which has an original grid spacing of 500 m (i.e., 64 GINA grid cells for every WRF grid cell). Interpolating 500-m GINA data to the 4-km WRF domain using a bilinear method may not have adequately smoothed the GINA dataset for a quantitative comparison. Regardless, the results clearly show that over most regions WRF has lower interannual variability than GINA for both FSD and LSD. Grid-averaged standard deviations in WRF are smaller by −5.07 days for FSD and −5.67 days for LSD (Table 2). Compared to OBS, the results are more mixed: WRF has both positive and negative differences with the OBS, though the lower variability in interior Alaska appears to be consistent.

e. *Evaluation of distributions of daily temperature, precipitation, and SWE*

WRF resolves the regional variations of daily 2-m temperature distributions for winter and summer compared to OBS (Figs. 9a,b). Median winter temperatures are colder in northern, western, and interior Alaska (regions 1–5) compared to the southern regions (6–13). Likewise, the highest summer temperatures, in the central and southern interior (regions 3 and 5) are simulated by WRF. Focusing in the interquartile range (IQR), WRF resolves the broader 2-m temperature distributions (higher daily variability) observed in winter compared to summer (note the different scales for winter versus summer 2-m temperature plots; if they were plotted on the same scales, the winter 2-m temperature ranges would appear even larger). WRF generally underestimates the overall maximum 2-m temperature in both seasons as indicated by the uppermost values of the distributions, which are the extreme values for each region over the entire 2002–16 record. In winter this extreme bias is modest (less than a few degrees Celsius) except in some southern coastal regions (8, 9, and 13), where the maximum 2-m temperature is underestimated by ~10°C. In summer, maximum 2-m temperatures are underestimated more widely. WRF accurately simulates the overall minimum winter 2-m temperature in the colder northern, western, and interior regions (1–5), but generally underestimates minima (i.e., is too warm) in the warmer southern coastal regions (7–12). WRF reasonably simulates summer minimum 2-m temperatures in general, with the exception of regions 7 and 8, where they are underestimated by >10°C. Given that median temperatures between WRF and OBS compare reasonably (suggesting no significant biases), without conducting specific case studies of extreme events (beyond the scope of this study), it is not presently clear why the overall 2-m temperature maxima and minima are underestimated in numerous regions. It may be partly due to influences of microclimate, elevation, and underlying land surface characteristics that are not resolved by the 16 km^2 grid cells in WRF. It is also possible that nuanced differences in the position and intensity of the storms that drive extremes (e.g., J. Cassano et al. 2016), and their interactions with local topography, lead to underestimates of their effects in WRF. Additionally, underestimated winter minima in the southern coastal regions may be related to a limited representation in WRF of temperature inversions in complex terrain (H. Zhang et al. 2013).

Prior to discussing the daily precipitation results in Figs. 9c,d, OBS and WRF precipitation days are compared across all Alaska sites for winter and summer (Table 3). WRF simulates precipitation for most days on which it is observed (83% in DJF and 87% in JJA). This result indicates that the choice to plot precipitation distributions in Figs. 9c,d only for days on which precipitation occurs in *both* OBS and WRF provides a representative distribution of observed precipitation (this choice was made because otherwise the precipitation results in both distributions are strongly skewed toward values of 0, obscuring key features). Table 3 also shows that WRF simulates about 70%–80% more precipitation days than are observed during both seasons. This issue of excessive simulated precipitation days is reduced to 8%–19% if only days on which precipitation > 1 mm are considered (not shown), indicating that the problem is largely due to WRF simulating trace amounts of precipitation (between 0 and 1 mm) on many days for which none is measured. This "drizzle" issue has been well documented across

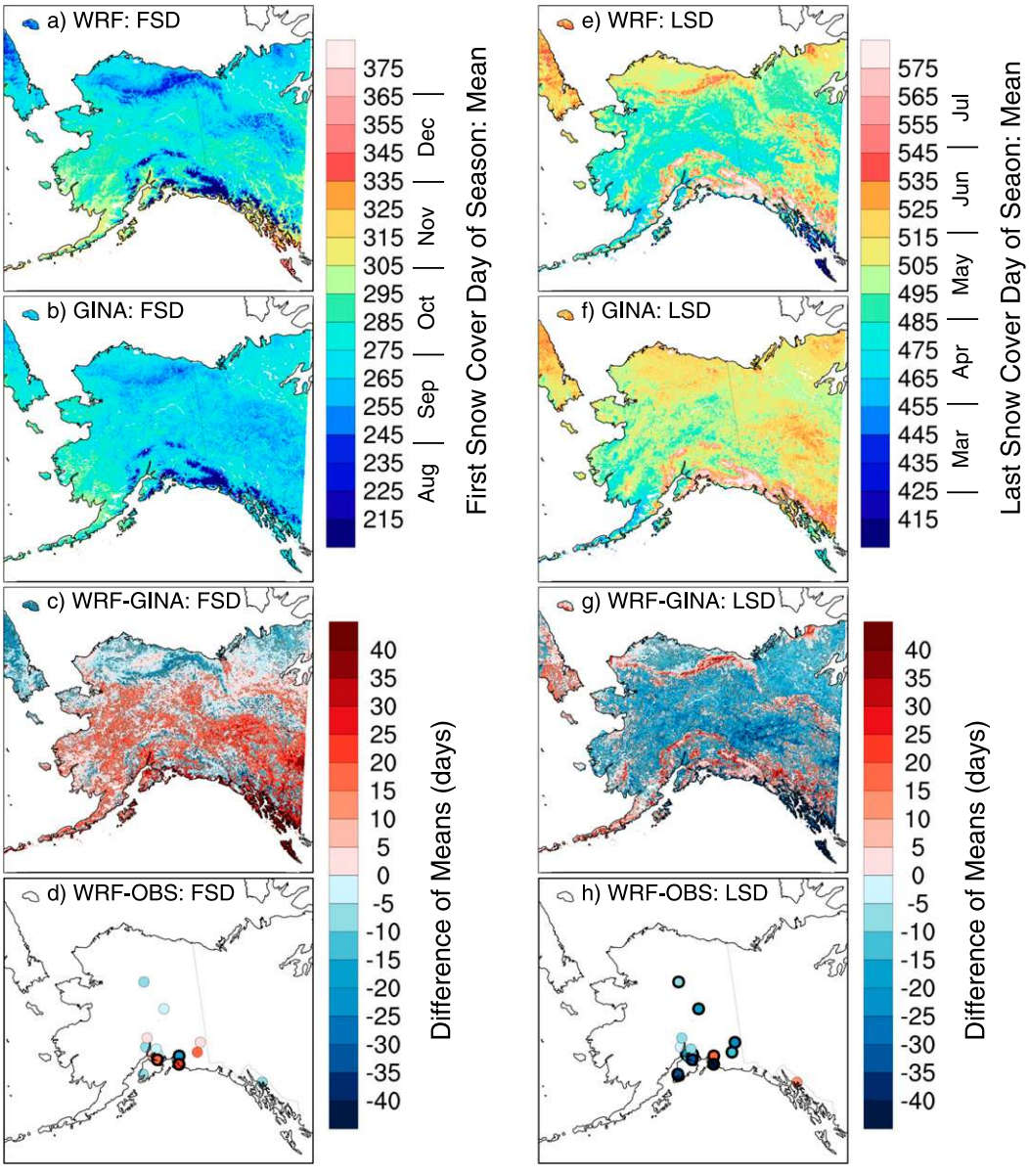

FIG. 7. Comparison of mean snow characteristics between WRF, GINA, and OBS. Shown are (a),(e) WRF 2004–16 means, (b),(f) GINA 2004–16 means, (c),(g) WRF minus GINA, and (d),(h) WRF minus OBS for the mean (left) FSD and (right) LSD. Statistically significant differences ($p < 0.05$) between WRF and GINA are outlined in thin gray contours in (c) and (g). Statistically significant differences between WRF and OBS are indicated by boldface-outlined circles in (d) and (h). The days of the snow season follow the convention used by Lindsay et al. (2015) and as described in the text.

numerous models (e.g., Sun et al. 2006). It may be partly related to the larger areal representation of the WRF grid cell (16 km^2) compared to a point-based observation, and to the inability of precipitation gauges to detect trace amounts of precipitation (Yang et al. 1998).

WRF broadly resolves the observed and simulated regional distributions of daily precipitation in winter and summer, as shown in Figs. 9c,d. The lowest winter precipitation amounts in both WRF and OBS occur in northern and interior Alaska (regions 1, 3, and 4) and the highest amounts in south-central and southeast Alaska (regions 10–13). Summer precipitation follows similar regional patterns in both WRF and OBS (Fig. 9d). Interestingly, in two adjacent regions in southeast Alaska—region 11 (the north panhandle) and region 12 (the central panhandle)—the observed precipitation amounts differ in terms of their seasonality. The precipitation is higher in winter than summer in the central panhandle,

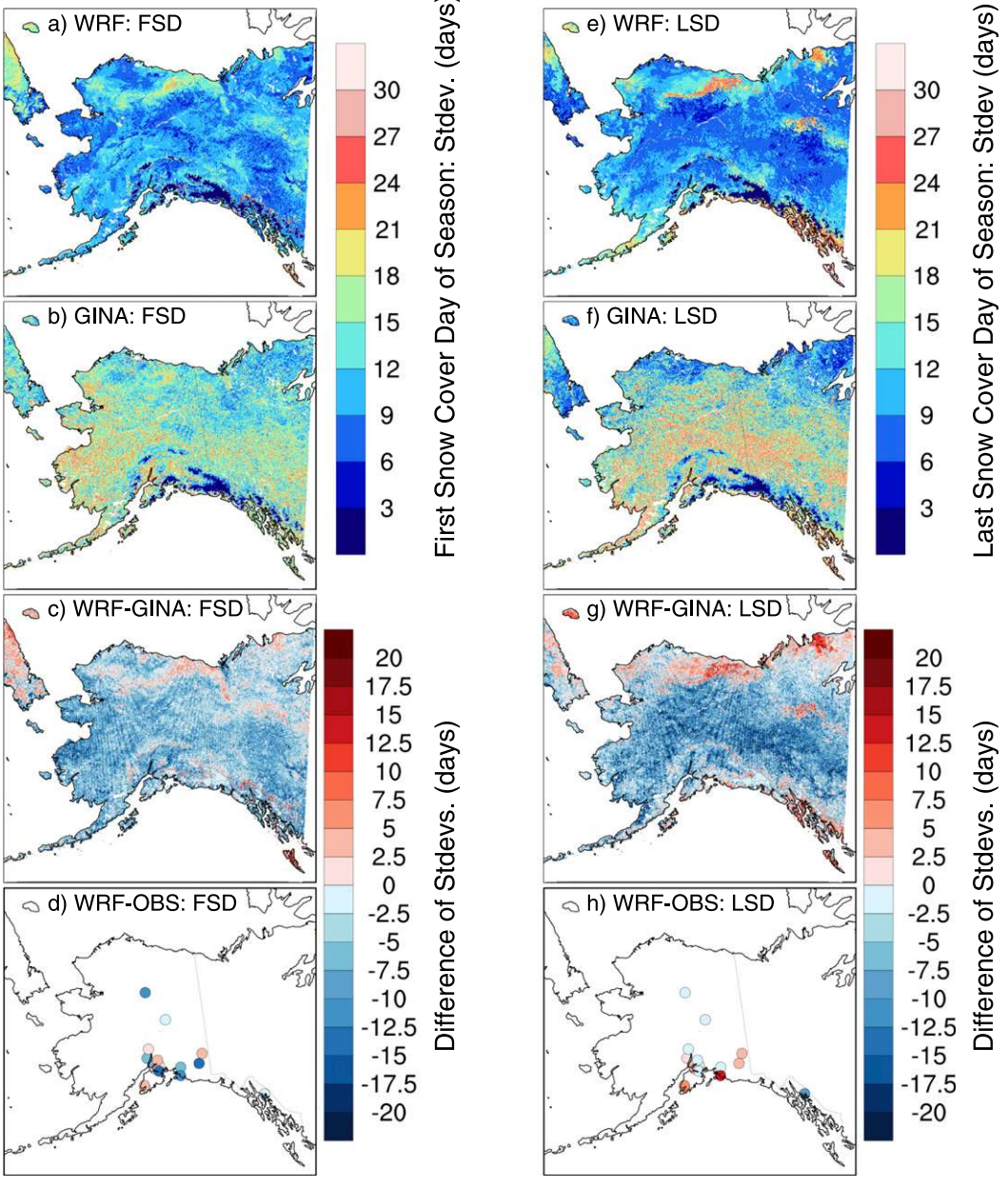

FIG. 8. Comparison of the standard deviation of mean snow characteristics between WRF, GINA, and OBS. Conventions are as in Fig. 7, with the exception that the statistical significance of differences cannot be computed.

whereas it is higher in summer than winter in the north panhandle; WRF resolves these observed differences. A winter low bias in median precipitation of approximately 0.5–3.0 mm day^{-1} is evident in northern, western and interior Alaska (regions 1–5), whereas in the higher-precipitation regions in south-central and southeastern Alaska (regions 10–13) the median precipitation is similar to observed. During summer there is a low bias in median precipitation in 12 of the 13 regions, although it is $<$1 mm day^{-1} in 7 of those regions. Possible reasons for precipitation biases are explored in section 4. Perhaps the most noteworthy result from Fig. 9 is that WRF accurately simulates the magnitude of the observed precipitation maxima in nearly every region during both seasons. This is a particularly important aspect because a major motivation for generating the WRF dataset is to investigate precipitation extremes.

To assess the annual cycle in WRF, weekly distributions of daily 2-m temperature, cumulative precipitation, and SWE were assessed along a north-to-south transect

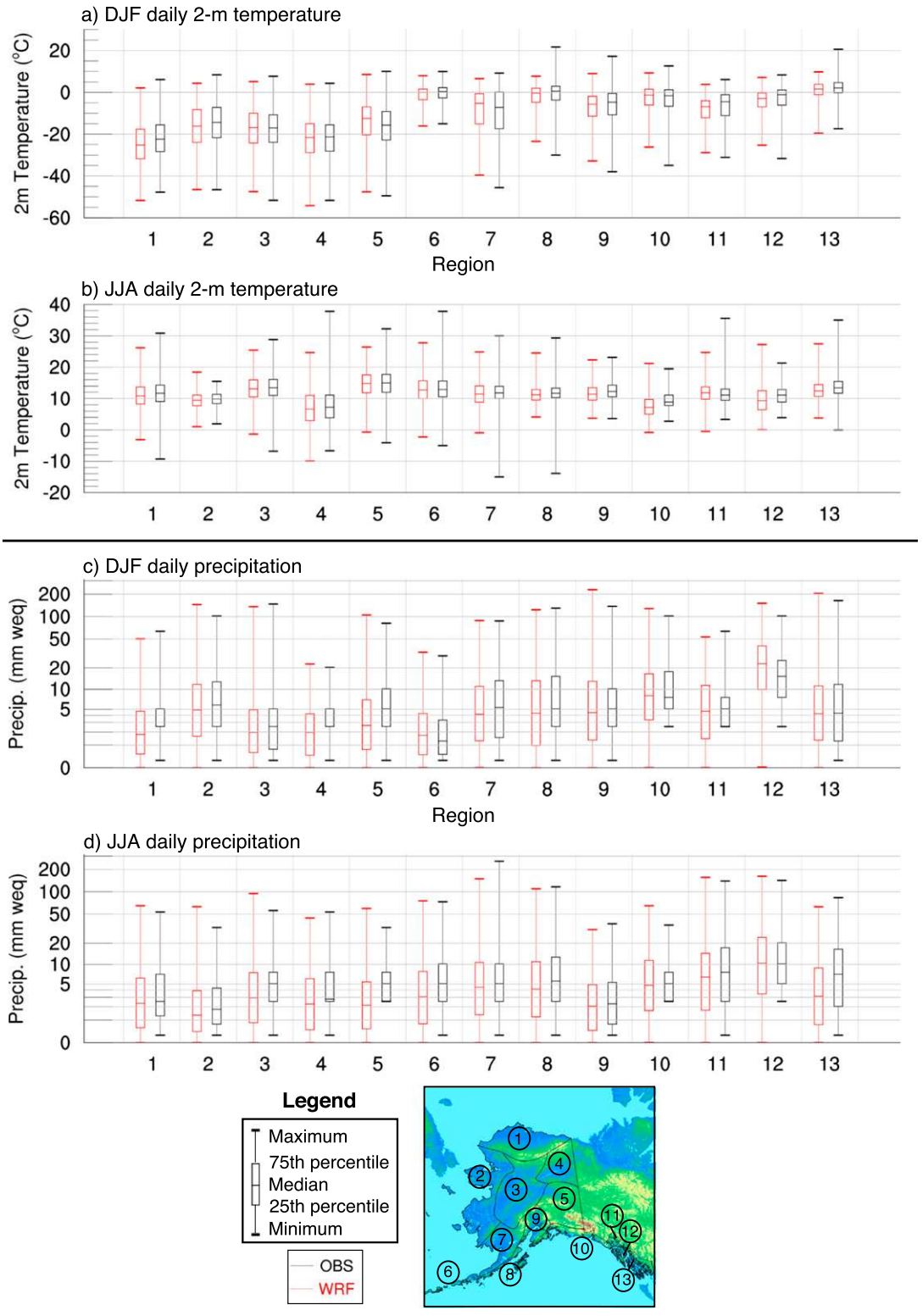

FIG. 9. WRF vs OBS daily (a),(b) 2-m air temperature and (c),(d) precipitation distributions for DJF and JJA, respectively, by Alaska climate region as indicated in the inset map. The plot was constructed by binning all available daily data from 2002 to 2016 by region and season and then calculating the minimum, 25th-percentile, median, 75th-percentile, and maximum values. Precipitation distributions are shown for days on which precipitation occurred in both OBS (black) and WRF (red). Days with no precipitation are not included.

of SNOTEL sites (Fig. 10). Site selection was based on balancing the quality and completeness of observed SWE records with geographical representativeness; for instance, Bettles is the most northerly site in Alaska for which there is a reliable SNOTEL SWE record. WRF simulates the broad distributions of daily 2-m temperature, for example the higher-amplitude annual cycle at the two northern sites. Winter warm biases on the order of 5°–10°C is evident at Bettles and of up to 5°C at Fairbanks, which persist into the spring months at both sites. While it is possible that winter cloud cover may play a role in biasing the longwave radiation balance at these sites, precipitation is accurately simulated, suggesting the simulated cloud cover is reasonable. Strong temperature inversions are common in interior Alaska (e.g., Malingowski et al. 2014), and it is more probable that WRF has a limited ability to simulate the strong temperature inversions that occur at both sites. This issue has contributed to warm biases in previous WRF studies over interior Alaska (Mölders and Kramm 2010; Hines et al. 2011). Additionally, positive incoming shortwave radiation biases may partially contribute to the warm biases during late winter and spring (see section 4). Maxima and minima of 2-m temperature are generally simulated accurately at the four sites, with the exception of winter at Bettles (where both maxima and minima are too warm), and winter at Cooper Lake (where maxima are too cold). The winter cold bias at Cooper Lake is also evident for median temperatures and may be partially due to the site being located at an elevation ~100 m higher in WRF. The weekly distributions of cumulative daily precipitation are simulated accurately in general, with WRF able to simulate maxima at the relatively low-precipitation sites of Bettles and Fairbanks. Maxima are overestimated at the two southern sites, and spring and summer precipitation is overestimated at Tokositna. The timing and magnitude of the annual cycle of SWE is simulated accurately at the interior sites, and the timing of the SWE cycle is simulated accurately at the southern sites, though the magnitudes are variable compared to OBS. An exception is that spring melt occurs too soon at all four sites, by about 2–4 weeks. This result is consistent with those presented above for WRF versus GINA, indicating that LSD in WRF occurs too early, and possible causes are discussed below.

4. Discussion and conclusions

Here, a new 14-yr (September 2002–August 2016) dataset for Alaska with 4-km grid spacing is described and evaluated. WRF 2-m air temperature, precipitation, and snowfall variables are evaluated at annual, seasonal, and daily time scales versus station records and observation-based, empirically derived gridded climate datasets that have similar grid spacing. The spatial patterns of the WRF fields compare well in nearly all cases to those in the gridded climate datasets; for example, the pattern correlations between annual mean WRF and observation-based gridded fields are $r = 0.89$ for 2-m temperature, $r = 0.75$ for precipitation, $r = 0.82$ for SDF, $r = 0.55$ for first snow day of the season, and $r = 0.71$ for last snow day of the season. The WRF dataset appears to have a more physically based representation of the interannual variability of 2-m temperature and precipitation compared to the observation-based gridded datasets, as shown in the analyses presented in Figs. 3 and 5. This may be expected, given that the gridded monthly meteorological anomaly fields in the CRU v3.1 dataset that SNAP is based on were computed from station observations using a triangular linear interpolation method (Harris et al. 2014), which may not fully depict geographically driven variability (e.g., due to orography and water bodies) when observational networks are sparse, as they are in Alaska. An additional strength of the WRF dataset is that it accurately depicts the magnitude of winter and summer precipitation maxima in regions throughout the state compared to station observations. This aspect bodes well for the subsequent use of the dataset for studies of precipitation extremes, a major motivation for conducting the simulations. The WRF dataset has a number of weaknesses, which are discussed below.

Perhaps the most important shortcoming of the WRF dataset is that spring snowmelt occurs too early over the majority of the state, due partly to positive 2-m temperature biases in winter that extend into the spring. The positive temperature biases may be linked to a number of issues, including 1) elevation differences between WRF and the evaluation datasets, 2) biases inherited from the ERA-Interim forcing dataset, 3) clear-sky incoming shortwave and longwave radiation biases (e.g., Hines and Bromwich 2008), 4) excessive cloudiness during winter (or conversely not enough clouds during spring when incoming shortwave radiation is substantial), or 5) other factors that might affect the energy balance such as the limited ability of WRF to handle extremely stable boundary layer conditions, which may in turn diminish simulations of temperature inversions (Mölders and Kramm 2010) [inadequate representation of inversions was also put forth by Bieniek et al. (2016) for 20-km WRF Alaska simulations]. While an exhaustive investigation of these possible factors is beyond the scope of this study, the first three factors are briefly addressed below. Factors 4 and 5 are explored in section3 (see the discussion of Fig. 10).

The first factor (elevation differences between WRF and evaluation datasets) is important at specific sites or

TABLE 3. Contingency table comparing the number of station days on which precipitation > 0 mm was observed (OBS) and simulated (WRF). Station-day statistics are aggregated across all Alaska stations for days on which data are nonmissing between September 2002 and August 2016.

		Event observed in OBS?			
		DJF		JJA	
		Yes	No	Yes	No
Event simulated by WRF?	Yes	20 027	21 329	23 862	25 367
	No	4176	28 028	3635	22 238

locally, particularly in the mountainous coastal areas, but tends to cancel out over larger regions. For example, the elevation difference between WRF and the station observations for the 164 sites analyzed ranges from −606 to +508 m, but the mean difference is only +20 m and the mean absolute difference is 98 m. The approximate temperature bias introduced by these elevation differences assuming a standard lapse rate (6.49°C km^{-1}) would be −0.13°C for the mean difference and ±0.63°C for the mean absolute difference. These values are noteworthy but are not adequate to substantially alter conclusions regarding the positive winter and spring temperature biases. Additionally, use of the standard lapse rate may provide a conservatively large estimate of bias introduced by elevation differences in high-latitude mountain regions (Marshall et al. 2007).

The second factor (inherited biases from ERA-Interim) does not appear to be a strong contributor to the WRF biases overall. Lader et al. (2016) compute the biases for ERA-Interim temperature versus the Hill et al. (2015) gridded observation-based dataset, which is similar to the SNAP dataset with which WRF is compared in Fig. 2. Their results indicate that the ERA-Interim 2-m temperature biases are not similar to those for WRF in Fig. 2 for either winter or summer. Notably, ERA-Interim has a cold bias over much of the Brooks Range and interior Alaska in winter, whereas WRF has a warm bias.

The third factor (the possibility of clear-sky radiation biases in WRF) was investigated by Hines and Bromwich (2008) for June 2001 over Greenland. They found that a polar-optimized version of WRF with the RRTM longwave scheme (which is used in this study) and the Goddard shortwave scheme simulated clear-sky incoming longwave radiation for the Summit station with minimal bias, suggesting excessive clear-sky longwave radiation may not be an issue in our simulations. However, they found a positive bias in incoming shortwave radiation. We investigated the possibility of a positive incoming shortwave radiation bias at radiation measurement sites in northern and interior Alaska using a WRF simulation that was conducted for 1 yr (September 2002–August 2003) as a precursor to the final 14-yr WRF simulation evaluated here. The precursor and final simulations had nearly identical model configurations. The results of the comparison (not shown) indicate that WRF incoming shortwave radiation along the North Slope (Barrow, Sagwon, Kuparuk, and Ivotuk) is nearly identical to OBS from February through April; in May, an important melt month, the incoming shortwave radiation in WRF is actually lower than observed. This is consistent with the 2-m temperature biases in that particular region, which are negative in WRF. However, at the interior site near Fairbanks, where there are strong positive 2-m temperature biases in winter and spring (Figs. 2 and 10), incoming shortwave radiation biases are positive in WRF from February through August. They are too large by ~30–40 W m^{-2} in the key melt months of April and May. It is thus possible that excessive incoming shortwave radiation during late winter and early spring contributes to warm biases during those seasons in interior Alaska, which in turn contribute to earlier-than-observed melt in WRF (Fig. 10). During sensitivity simulations in preparation for our production runs we attempted to mitigate the early melt bias by optimizing Noah-MP to retain snowpack during warm periods (see section 2); however this effort appears to have been only partially successful.

An additional shortcoming of the WRF dataset is the existence of positive precipitation biases over the lower-elevation regions of interior and northern Alaska, and negative precipitation biases over the Pacific Coast Ranges in southern Alaska, in both winter and summer. This conclusion is primarily based on comparison to the SNAP precipitation fields, and is not as pronounced in comparison to the few precipitation observations that exist (Fig. 4). Therefore, the differences may be partially attributed to biases in SNAP. SNAP employs PRISM precipitation fields to inform its background state. In turn, the lapse rates that are used in the PRISM interpolation method may be uncertain in areas where there are few measurements to provide constraint (Daly et al. 1994), particularly in complex terrain (Henn et al. 2017). It is also noteworthy that the 20-km WRF simulations evaluated by Bieniek et al. (2016) were subject to these same bias patterns. They posited that the positive biases might be partly due to observational uncertainty, particularly gauge undercatch during winter. They also noted that the quality and magnitude of precipitation in mountainous areas is difficult to assess because most observation sites are located at low elevations. Moreover, in some areas point-based observations may not be representative of the 16 km^2 WRF grid cells. Finally, Bieniek et al. (2016) noted that ERA-Interim, which they also used for the boundary conditions for WRF, has overall positive precipitation biases compared to observations (Lader et al.

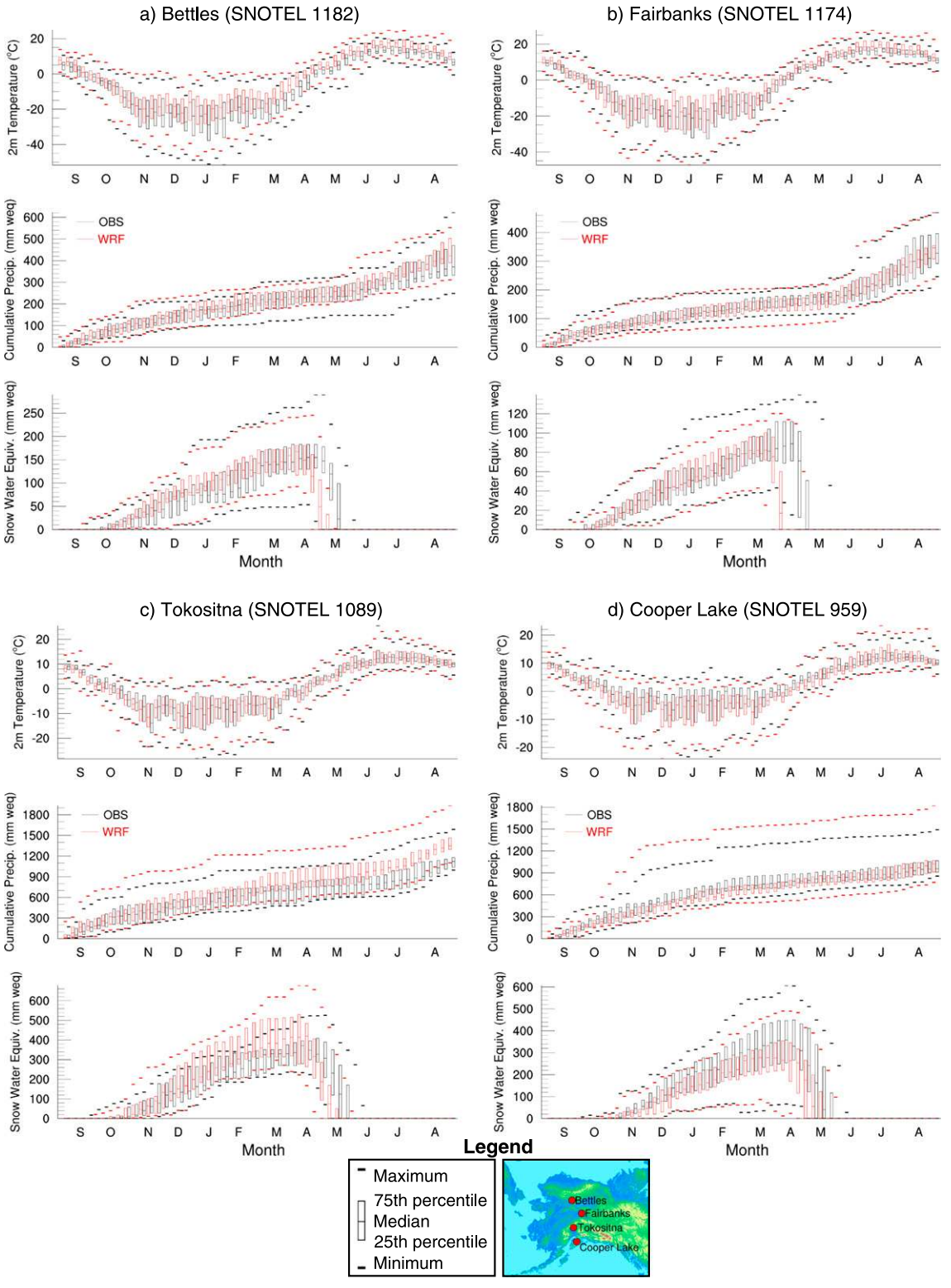

FIG. 10. WRF vs SNOTEL annual cycle of 2-m air temperature, cumulative precipitation, and SWE at four sites along the north-to-south transect indicated in the inset map. The plot was constructed by binning all available daily data from 2002 to 2016 by week of year and then calculating the minimum, 25th-percentile, median, 75th-percentile, and maximum values.

2016), raising the possibility that excessive moisture may be propagated through the WRF boundaries.

Despite the limitations noted above, this initial evaluation suggests the 4-km WRF climate dataset robustly simulates meteorological processes and recent climatic variability in Alaska. Future studies will provide further insight on its ability to represent specific aspects of Alaska climate. The new dataset should be viewed as an additional resource for the community that, when used in conjunction with other data sources, can enhance our understanding of the spatiotemporal variability of Alaska's weather and climate. The ability of the dataset to resolve year-to-year meteorological variability and precipitation maxima at comparatively high spatial resolution make it particularly well suited for studies of extreme events and the processes that drive them, in addition to its potential utility for driving other models (e.g., hydrologic or glacier models), or studying the diurnal cycle. The WRF fields may also be useful for informing the background spatial and temporal variability for the creation of new observation-based, empirically derived gridded climate products. Selected meteorological fields from the WRF dataset are presently available to the community at a variety of time scales (Monaghan et al. 2016).

Acknowledgments. This research is funded by the U.S. Army Corps of Engineers National Climate Preparedness and Resilience Program and sponsored by the National Science Foundation (NSF). Computing resources (ark:/85065/d7wd3xhc) on the National Center for Atmospheric Research (NCAR) Yellowstone system were granted via an NCAR Strategic Capability allocation and were provided by NCAR's Computational and Information Systems Laboratory, sponsored by NSF and other agencies. NCAR is sponsored by NSF. The authors thank Greg Thompson for providing an early-release bug fix for the Thompson microphysics scheme. Ethan Gutman, Keith Musselman, and Changhai Liu provided insightful comments during the planning stages.

REFERENCES

Balshi, M. S., A. D. McGuire, P. Duffy, M. Flannigan, J. Walsh, and J. Melillo, 2009: Assessing the response of area burned to changing climate in western boreal North America using a Multivariate Adaptive Regression Splines (MARS) approach. *Global Change Biol.*, **15**, 578–600, https://doi.org/10.1111/j.1365-2486.2008.01679.x.

Barnhart, K. R., R. S. Anderson, I. Overeem, C. Wobus, G. D. Clow, and F. E. Urban, 2014: Modeling erosion of ice-rich permafrost bluffs along the Alaskan Beaufort Sea coast. *J. Geophys. Res. Earth Surf.*, **119**, 1155–1179, https://doi.org/10.1002/2013JF002845.

Beamer, J. P., D. F. Hill, A. Arendt, and G. E. Liston, 2016: High-resolution modeling of coastal freshwater discharge and glacier mass balance in the Gulf of Alaska watershed. *Water Resour. Res.*, **52**, 3888–3909, https://doi.org/10.1002/2015WR018457.

Bennett, K. E., A. J. Cannon, and L. Hinzman, 2015: Historical trends and extremes in boreal Alaska river basins. *J. Hydrol.*, **527**, 590–607, https://doi.org/10.1016/j.jhydrol.2015.04.065.

Bieniek, P. A., and Coauthors, 2012: Climate divisions for Alaska based on objective methods. *J. Appl. Meteor. Climatol.*, **51**, 1276–1289, https://doi.org/10.1175/JAMC-D-11-0168.1.

——, J. E. Walsh, R. L. Thoman, and U. S. Bhatt, 2014: Using climate divisions to analyze variations and trends in Alaska temperature and precipitation. *J. Climate*, **27**, 2800–2818, https://doi.org/10.1175/JCLI-D-13-00342.1.

——, and Coauthors, 2015: Climate drivers linked to changing seasonality of Alaska coastal tundra vegetation productivity. *Earth Interact.*, **19**, https://doi.org/10.1175/EI-D-15-0013.1.

——, U. S. Bhatt, J. E. Walsh, T. S. Rupp, J. Zhang, J. R. Krieger, and R. Lader, 2016: Dynamical downscaling of ERA-Interim temperature and precipitation for Alaska. *J. Appl. Meteor. Climatol.*, **55**, 635–654, https://doi.org/10.1175/JAMC-D-15-0153.1.

Bromwich, D. H., A. B. Wilson, L.-S. Bai, G. W. K. Moore, and P. Bauer, 2016: A comparison of the regional Arctic System Reanalysis and the global ERA-Interim reanalysis for the Arctic. *Quart. J. Roy. Meteor. Soc.*, **142**, 644–658, https://doi.org/10.1002/qj.2527.

Brubaker, M. Y., J. N. Bell, J. E. Berner, and J. A. Warren, 2011: Climate change health assessment: A novel approach for Alaska native communities. *Int. J. Circumpolar Health*, **70**, 266–273, https://doi.org/10.3402/ijch.v70i3.17820.

Cassano, E. N., J. J. Cassano, and M. Nolan, 2011: Synoptic weather pattern controls on temperature in Alaska. *J. Geophys. Res.*, **116**, D11108, https://doi.org/10.1029/2010JD015341.

——, ——, M. W. Seefeldt, W. J. Gutowski, and J. M. Glisan, 2016: Synoptic conditions during summertime temperature extremes in Alaska. *Int. J. Climatol.*, **37**, 3694–3713, https://doi.org/10.1002/joc.4949.

Cassano, J. J., M. E. Higgins, and M. W. Seefeldt, 2011: Performance of the Weather Research and Forecasting Model for month-long pan-Arctic simulations. *Mon. Wea. Rev.*, **139**, 3469–3488, https://doi.org/10.1175/MWR-D-10-05065.1.

——, E. N. Cassano, M. W. Seefeldt, W. J. Gutowski, and J. M. Glisan, 2016: Synoptic conditions during wintertime temperature extremes in Alaska. *J. Geophys. Res. Atmos.*, **121**, 3241–3262, https://doi.org/10.1002/2015JD024404.

Dai, A., 2008: Temperature and pressure dependence of the rain-snow phase transition over land and ocean. *Geophys. Res. Lett.*, **35**, L12802, https://doi.org/10.1029/2008GL033295.

Daly, C., R. P. Neilson, and D. L. Phillips, 1994: A statistical–topographic model for mapping climatological precipitation over mountainous terrain. *J. Appl. Meteor.*, **33**, 140–158, https://doi.org/10.1175/1520-0450(1994)033<0140:ASTMFM>2.0.CO;2.

Dee, D. P., and Coauthors, 2011: The ERA-Interim reanalysis: Configuration and performance of the data assimilation system. *Quart. J. Roy. Meteor. Soc.*, **137**, 553–597, https://doi.org/10.1002/qj.828.

Derksen, C., and R. Brown, 2012: Spring snow cover extent reductions in the 2008–2012 period exceeding climate model projections. *Geophys. Res. Lett.*, **39**, L19504, https://doi.org/10.1029/2012GL053387.

Durre, I., M. J. Menne, B. E. Gleason, T. G. Houston, and R. S. Vose, 2010: Comprehensive automated quality assurance of daily surface observations. *J. Appl. Meteor. Climatol.*, **49**, 1615–1633, https://doi.org/10.1175/2010JAMC2375.1.

DuVivier, A. K., J. J. Cassano, A. Craig, J. Hamman, W. Maslowski, B. Nijssen, R. Osinski, and A. Roberts, 2016: Winter atmospheric

buoyancy forcing and oceanic response during strong wind events around southeastern Greenland in the Regional Arctic System Model (RASM) for 1990–2010. *J. Climate*, **29**, 975–994, https://doi.org/10.1175/JCLI-D-15-0592.1.

Fleming, M. D., F. S. Chapin, W. Cramer, G. L. Hufford, and M. C. Serreze, 2000: Geographic patterns and dynamics of Alaskan climate interpolated from a sparse station record. *Global Change Biol.*, **6**, 49–58, https://doi.org/10.1046/j.1365-2486.2000.06008.x.

Friedl, M. A., and Coauthors, 2002: Global land cover mapping from MODIS: Algorithms and early results. *Remote Sens. Environ.*, **83**, 287–302, https://doi.org/10.1016/S0034-4257(02)00078-0.

Gesch, D., and S. Greenlee, 1999: GTOPO30 documentation. U.S. Geological Survey, https://webgis.wr.usgs.gov/globalgis/gtopo30/gtopo30.htm.

GINA, 2016: MODIS-derived snow metrics. Geographic Information Network of Alaska, http://www.gina.alaska.edu/projects/modis-derived-snow-metrics.

Glisan, J. M., W. J. Gutowski, J. J. Cassano, E. N. Cassano, and M. W. Seefeldt, 2016: Analysis of WRF extreme daily precipitation over Alaska using self-organizing maps. *J. Geophys. Res. Atmos.*, **121**, 7746–7761, https://doi.org/10.1002/2016JD024822.

Gong, W., F. J. Meyer, P. Webley, and D. Morton, 2013: Performance of the high-resolution atmospheric model HRRR-AK for correcting geodetic observations from spaceborne radars. *J. Geophys. Res. Atmos.*, **118**, 11 611–11 624, https://doi.org/10.1002/2013JD020170.

Goudriaan, J., 1985: *Crop Micrometeorology: A Simulation Study* (in Dutch). *Simulation Monogr.*, Wageningen University, 249 pp., http://edepot.wur.nl/166537.

Harris, I., P. D. Jones, T. J. Osborn, and D. H. Lister, 2014: Updated high-resolution grids of monthly climatic observations—The CRU TS3.10 dataset. *Int. J. Climatol.*, **34**, 623–642, https://doi.org/10.1002/joc.3711.

Henn, B., A. J. Newman, B. Livneh, C. Daly, and J. D. Lundquist, 2017: An assessment of differences in gridded precipitation datasets in complex terrain. *J. Hydrol.*, **556**, 1205–1219, https://doi.org/10.1016/j.jhydrol.2017.03.008.

Hill, D. F., N. Bruhis, S. E. Calos, A. Arendt, and J. Beamer, 2015: Spatial and temporal variability of freshwater discharge into the Gulf of Alaska. *J. Geophys. Res. Oceans*, **120**, 634–646, https://doi.org/10.1002/2014JC010395.

Hines, K. M., and D. H. Bromwich, 2008: Development and testing of Polar Weather Research and Forecasting (WRF) Model. Part I: Greenland ice sheet meteorology. *Mon. Wea. Rev.*, **136**, 1971–1989, https://doi.org/10.1175/2007MWR2112.1.

——, ——, L.-S. Bai, M. Barlage, and A. G. Slater, 2011: Development and testing of Polar WRF. Part III: Arctic land. *J. Climate*, **24**, 26–48, https://doi.org/10.1175/2010JCLI3460.1.

Hinzman, L. D., and Coauthors, 2005: Evidence and implications of recent climate change in northern Alaska and other Arctic regions. *Climatic Change*, **72**, 251–298, https://doi.org/10.1007/s10584-005-5352-2.

Johnson, J. B., A. Gelvin, and G. Schaefer, 2007: An engineering design study of electronic snow water equivalent sensor performance. *75th Annual Western Snow Conf.,* Kailua-Kona, HI, Western Snow Conference, 16–19, https://westernsnowconference.org/sites/westernsnowconference.org/PDFs/2007Johnson.pdf.

Jones, P. D., 1994: Hemispheric surface air temperature variations: A reanalysis and an update to 1993. *J. Climate*, **7**, 1794–1802, https://doi.org/10.1175/1520-0442(1994)007<1794:HSATVA>2.0.CO;2.

Kane, D. L., and S. L. Stuefer, 2015: Reflecting on the status of precipitation data collection in Alaska: A case study. *Hydrol. Res.*, **46**, 478–493, https://doi.org/10.2166/nh.2014.023.

Kienzle, S. W., 2008: A new temperature based method to separate rain and snow. *Hydrol. Processes*, **22**, 5067–5085, https://doi.org/10.1002/hyp.7131.

Klemp, J. B., W. C. Skamarock, and J. Dudhia, 2007: Conservative split-explicit time integration methods for the compressible nonhydrostatic equations. *Mon. Wea. Rev.*, **135**, 2897–2913, https://doi.org/10.1175/MWR3440.1.

Lader, R., U. S. Bhatt, J. E. Walsh, T. S. Rupp, and P. A. Bieniek, 2016: Two-meter temperature and precipitation from atmospheric reanalysis evaluated for Alaska. *J. Appl. Meteor. Climatol.*, **55**, 901–922, https://doi.org/10.1175/JAMC-D-15-0162.1.

Lindsay, C., J. Zhu, A. E. Miller, P. Kirchner, and T. L. Willson, 2015: Deriving snow cover metrics for Alaska from MODIS. *Remote Sens.*, **7**, 12 961–12 985, https://doi.org/10.3390/rs71012961.

Lindsay, R., M. Wensnahan, A. Schweiger, and J. Zhang, 2014: Evaluation of seven different atmospheric reanalysis products in the Arctic. *J. Climate*, **27**, 2588–2606, https://doi.org/10.1175/JCLI-D-13-00014.1.

Liu, F., J. R. Krieger, and J. Zhang, 2014: Toward producing the Chukchi–Beaufort High-Resolution Atmospheric Reanalysis (CBHAR) via the WRFDA data assimilation system. *Mon. Wea. Rev.*, **142**, 788–805, https://doi.org/10.1175/MWR-D-13-00063.1.

Lorenz, C., and H. Kunstmann, 2012: The hydrological cycle in three state-of-the-art reanalyses: Intercomparison and performance analysis. *J. Hydrometeor.*, **13**, 1397–1420, https://doi.org/10.1175/JHM-D-11-088.1.

Malingowski, J., D. Atkinson, J. Fochesatto, J. Cherry, and E. Stevens, 2014: An observational study of radiation temperature inversions in Fairbanks, Alaska. *Polar Sci.*, **8**, 24–39, https://doi.org/10.1016/j.polar.2014.01.002.

Mallard, M. S., C. G. Nolte, O. R. Bullock, T. L. Spero, and J. Gula, 2014: Using a coupled lake model with WRF for dynamical downscaling. *J. Geophys. Res. Atmos.*, **119**, 7193–7208, https://doi.org/10.1002/2014JD021785.

Markon, C. J., S. F. Trainor, and F. S. Chapin III, Eds., 2012: The United States National Climate Assessment—Alaska technical regional report. U.S. Geological Survey Circular 1379, 148 pp., http://pubs.er.usgs.gov/publication/cir1379.

Marshall, S. J., M. J. Sharp, D. O. Burgess, and F. S. Anslow, 2007: Near-surface-temperature lapse rates on the Prince of Wales Icefield, Ellesmere Island, Canada: Implications for regional downscaling of temperature. *Int. J. Climatol.*, **27**, 385–398, https://doi.org/10.1002/joc.1396.

McAfee, S. A., G. Guentchev, and J. K. Eischeid, 2013: Reconciling precipitation trends in Alaska: 1. Station-based analyses. *J. Geophys. Res. Atmos.*, **118**, 7523–7541, https://doi.org/10.1002/jgrd.50572.

——, ——, and J. Eischeid, 2014a: Reconciling precipitation trends in Alaska: 2. Gridded data analyses. *J. Geophys. Res. Atmos.*, **119**, 13 820–13 837, https://doi.org/10.1002/2014JD022461.

——, J. Walsh, and T. S. Rupp, 2014b: Statistically downscaled projections of snow/rain partitioning for Alaska. *Hydrol. Processes*, **28**, 3930–3946, https://doi.org/10.1002/hyp.9934.

Melvin, A. M., J. Murray, B. Boehlert, J. A. Martinich, L. Rennels, and T. S. Rupp, 2017: Estimating wildfire response costs in Alaska's changing climate. *Climatic Change*, **141**, 783–795, https://doi.org/10.1007/s10584-017-1923-2.

Menne, M. J., and Coauthors, 2012a: Global Historical Climatology Network - Daily (GHCN-Daily), version 3.22. National Centers for Environmental Information, accessed 1 August 2016, https://doi.org/10.7289/V5D21VHZ.

——, I. Durre, R. S. Vose, B. E. Gleason, and T. G. Houston, 2012b: An overview of the Global Historical Climatology

Network-Daily database. *J. Atmos. Oceanic Technol.*, **29**, 897–910, https://doi.org/10.1175/JTECH-D-11-00103.1.

Mölders, N., and G. Kramm, 2010: A case study on wintertime inversions in interior Alaska with WRF. *Atmos. Res.*, **95**, 314–332, https://doi.org/10.1016/j.atmosres.2009.06.002.

Monaghan, A. J., M. P. Clark, M. P. Barlage, A. J. Newman, L. Xue, J. R. Arnold, and R. M. Rasmussen, 2016: High-resolution climate simulations over Alaska: A community dataset, version 1. National Center for Atmospheric Research Earth System Grid, accessed 1 December 2016, https://doi.org/10.5065/D61Z42T0.

NASA JPL, 2015: GHRSST Level 4 MUR Global Foundation Sea Surface Temperature Analysis (v4.1). NASA Jet Propulsion Laboratory, accessed 30 October 2016, https://doi.org/10.5067/GHGMR-4FJ04.

Niu, G.-Y., and Z.-L. Yang, 2007: An observation-based formulation of snow cover fraction and its evaluation over large North American river basins. *J. Geophys. Res.*, **112**, D21101, https://doi.org/10.1029/2007JD008674.

——, and Coauthors, 2011: The community Noah land surface model with multiparameterization options (Noah-MP): 1. Model description and evaluation with local-scale measurements. *J. Geophys. Res.*, **116**, D12109, https://doi.org/10.1029/2010JD015139.

NOAA/NCEI, 2016: Global surface summary of the day. National Centers for Environmental Information, ftp://ftp.ncdc.noaa.gov/pub/data/gsod.

NRCS, 2016: All sensors—SNOTEL data. National Resources Conservation Service, http://www.wcc.nrcs.usda.gov/snow/snotel-data.html.

——, 2017: Snow surveys and water supply forecasting. National Resources Conservation Service, https://www.wcc.nrcs.usda.gov/factpub/sect_4b.html.

Park, T., and Coauthors, 2016: Changes in growing season duration and productivity of northern vegetation inferred from long-term remote sensing data. *Environ. Res. Lett.*, **11**, 084001, https://doi.org/10.1088/1748-9326/11/8/084001.

Prein, A. F., G. J. Holland, R. M. Rasmussen, J. Done, K. Ikeda, M. P. Clark, and C. H. Liu, 2013: Importance of regional climate model grid spacing for the simulation of heavy precipitation in the Colorado headwaters. *J. Climate*, **26**, 4848–4857, https://doi.org/10.1175/JCLI-D-12-00727.1.

Rasmussen, R., and Coauthors, 2011: High-resolution coupled climate runoff simulations of seasonal snowfall over Colorado: A process study of current and warmer climate. *J. Climate*, **24**, 3015–3048, https://doi.org/10.1175/2010JCLI3985.1.

Rattenbury, K., K. Kielland, G. Finstad, and W. Schneider, 2009: A reindeer herder's perspective on caribou, weather and socio-economic change on the Seward Peninsula, Alaska. *Polar Res.*, **28**, 71–88, https://doi.org/10.1111/j.1751-8369.2009.00102.x.

Sampson, G. R., and T. L. Wurtz, 1994: Record interior Alaska snowfall effect on tree breakage. *N. J. Appl. For.*, **11**, 138–140.

Schaefer, G. L., and R. F. Paetzold, 2000: SNOTEL (SNOwpack TELemetry) and SCAN (soil climate analysis network). *Automated Weather Stations for Applications in Agriculture and Water Resources Management: Current Use and Future*, AGM-3 and WMO/TD-1074, K. G. Hubbard and M. V. K. Sivakumar, Eds., World Meteorological Organization, 256 pp., http://www.wamis.org/agm/pubs/agm3/WMO-TD1074.pdf.

Shulski, M., J. Walsh, E. Stevens, and R. Thoman, 2010: Diagnosis of extended cold-season temperature anomalies in Alaska. *Mon. Wea. Rev.*, **138**, 453–462, https://doi.org/10.1175/2009MWR3039.1.

Simpson, J. J., G. L. Hufford, M. D. Fleming, J. S. Berg, and J. B. Ashton, 2002: Long-term climate patterns in Alaskan surface temperature and precipitation and their biological consequences. *IEEE Trans. Geosci. Remote Sens.*, **40**, 1164–1184, https://doi.org/10.1109/TGRS.2002.1010902.

——, ——, C. Daly, J. S. Berg, and M. D. Fleming, 2005: Comparing maps of mean monthly surface temperature and precipitation for Alaska and adjacent areas of Canada produced by two different methods. *Arctic*, **58**, 137–161.

Skamarock, W. C., and J. B. Klemp, 2008: A time-split nonhydrostatic atmospheric model for weather research and forecasting applications. *J. Comput. Phys.*, **227**, 3465–3485, https://doi.org/10.1016/j.jcp.2007.01.037.

——, and Coauthors, 2008: A description of the Advanced Research WRF version 3. NCAR Tech. Note NCAR/TN-475+STR, 113 pp., http://dx.doi.org/10.5065/D68S4MVH.

SNAP, 2016: Scenarios Network for Alaska and Arctic Planning Data. University of Alaska Fairbanks, accessed 1 August 2016, http://ckan.snap.uaf.edu/dataset.

Stafford, J. M., G. Wendler, and J. Curtis, 2000: Temperature and precipitation of Alaska: 50 year trend analysis. *Theor. Appl. Climatol.*, **67**, 33–44, https://doi.org/10.1007/s007040070014.

Stone, R. S., E. G. Dutton, J. M. Harris, and D. Longenecker, 2002: Earlier spring snowmelt in northern Alaska as an indicator of climate change. *J. Geophys. Res.*, **107**, https:/doi.org/10.1029/2000JD000286.

Sun, Y., S. Solomon, A. Dai, and R. W. Portmann, 2006: How often does it rain? *J. Climate*, **19**, 916–934, https://doi.org/10.1175/JCLI3672.1.

Sundqvist, H., E. Berge, and J. E. Kristjánsson, 1989: Condensation and cloud parameterization studies with a mesoscale numerical weather prediction model. *Mon. Wea. Rev.*, **117**, 1641, https:/doi.org/10.1175/1520-0493(1989)117<1641:CACPSW>2.0.CO;2.

Walsh, J. E., 2014: Intensified warming of the Arctic: Causes and impacts on middle latitudes. *Global Planet. Change*, **117**, 52–63, https://doi.org/10.1016/j.gloplacha.2014.03.003.

——, P. A. Bieniek, B. Brettschneider, E. S. Euskirchen, R. Lader, and R. L. Thoman, 2017: The exceptionally warm winter of 2015/16 in Alaska. *J. Climate*, **30**, 2069–2088, https://doi.org/10.1175/JCLI-D-16-0473.1.

Wendler, G., and M. Shulski, 2009: A century of climate change for Fairbanks, Alaska. *Arctic*, **62**, 295–300, https://doi.org/10.14430/arctic149.

Yang, D., B. E. Goodison, J. R. Metcalfe, V. S. Golubev, R. Bates, T. Pangburn, and C. L. Hanson, 1998: Accuracy of NWS 8'' standard nonrecording precipitation gauge: Results and application of WMO intercomparison. *J. Atmos. Oceanic Technol.*, **15**, 54–68, https://doi.org/10.1175/1520-0426(1998)015<0054:AONSNP>2.0.CO;2.

Zhang, H., Z. Pu, and X. Zhang, 2013: Examination of errors in near-surface temperature and wind from WRF numerical simulations in regions of complex terrain. *Wea. Forecasting*, **28**, 893–914, https://doi.org/10.1175/WAF-D-12-00109.1.

Zhang, J., U. S. Bhatt, W. V. Tangborn, and C. S. Lingle, 2007: Climate downscaling for estimating glacier mass balances in northwestern North America: Validation with a USGS benchmark glacier. *Geophys. Res. Lett.*, **34**, L21505, https://doi.org/10.1029/2007GL031139.

Zhang, X., and Coauthors, 2013: Beaufort and Chukchi Seas Mesoscale Meteorology Modeling Study: Final project report. Bureau of Ocean Energy Management Rep. 2013-0119, 204 pp., https://www.boem.gov/BOEM-2013-0119.